A Micromechanical Biosensor with Inherently Differential Readout

by

Cagri Abdullah Savran

B.S. Mechanical Engineering
Purdue University 1998
S.M. Mechanical Engineering
Massachusetts Institute of Technology 2000

Submitted to the Department of Mechanical Engineering
in partial fulfillment of the requirements for the degree of

Doctor of Philosophy

at the

MASSACHUSETTS INSTITUTE OF TECHNOLOGY

February 2004

Signature redacted

Author .....
Department of Mechanical Engineering
December 18, 2003

Certified by.... Signature redacted .....
Scott R. Manalis
Associate Professor of Biological Engineering, and Media Arts and Sciences
Thesis Supervisor

Certified by..... Signature redacted .....
Alexander H. Slocum
Professor of Mechanical Engineering
Committee Chair

Accepted by..... Signature redacted .....
Ain Sonin
Chairman, Department Committee on Graduate Students

A Micromechanical Biosensor with Inherently Differential Readout

by

Cagri Abdullah Savran

Submitted to the Department of Mechanical Engineering
on December 18, 2003, in partial fulfillment of the
requirements for the degree of
Doctor of Philosophy

Abstract

The ability to detect biomolecules in real-time and without the use of labels has significant benefits for systems biology in terms of cost, time and throughput. Cantilever-based micromechanical sensors detect biomolecular adsorption by means of surface-stress-induced cantilever bending. This technique enables sensitive, scalable and label-free detection of biomolecules in real-time. However, micromachined cantilevers are extremely sensitive to nonspecific chemical effects and temperature changes. This thesis explores a micromechanical sensor that suppresses disturbances by generating an inherently differential signal with respect to a reference surface. The thesis covers the design, fabrication, characterization of the sensor, and its application to protein detection using *aptamers*; receptor molecules produced *in vitro*.

The sensor is composed of two adjacent cantilevers that form a sensor-reference pair, whereby only the sensing surface is activated with receptor molecules that are specific to the ligand to be detected. The relative, or differential bending between the two cantilevers is directly measured using interferometry. Through direct differential detection, disturbances affecting both cantilevers are suppressed at the measurement level. This eliminates the need for separate detection of each cantilever's motion and off-line processing of the individual signals.

At high frequencies, the resolution of the sensor is only limited by its sub-angstrom-level thermomechanical noise. At lower frequencies (frequencies of interest), the resolution is limited by $1/f$-type noise which can be reduced by as much as an order of magnitude by direct differential detection, enabling clear observation of receptor-ligand binding reactions in real-time.

Thesis Supervisor: Scott R. Manalis
Title: Associate Professor of Biological Engineering, and Media Arts and Sciences

Acknowledgments

I would like to thank all my colleagues at the MIT Nanoscale Sensing Group without whose help, this thesis study would suffer greatly. Andrew Sparks gets special thanks for providing expertise in microfabrication because *he is a good man, and thorough.* Emily Cooper, Maxim Shusteff, and Nin Loh get special thanks for all their help and patience. Jurgen Fritz, a.k.a. *the good doktore* played the most important role in my understanding of cantilever-bases sensors and functionalization processes. Thomas Burg's indispensable and heroic effort in the improvement of the experimental setup deserves most profound thanks.

I thank my advisor Prof. Scott Manalis for his guidance, expertise, support, understanding, and showing me the hot spots of San Francisco. My most profound thanks go to Prof. Steve Senturia for being in my committee and providing expertise in the area of MEMS. *I agree with Professor Senturia!* (God help you, if you don't.) Prof. Alex Slocum has provided invaluable comments and support throughout my thesis study. I would also like to thank Prof. Marty Schmidt for providing expertise in the area of microfabrication. Vicky Diadiuk, Kurt Broderick and Jim Bishop of the MIT Microsystems Technology Laboratories get very special thanks for their help.

I thank my friend Prof. Bayram Tekin for teaching me physics, and arranging vivid discussions. I owe a lot to my friend Fatih Yanik who has encouraged me to get into MEMS, when I was working on much larger structures. I thank my friend Ertugrul Ozbudak for his indispensable contributions to my efforts in learning biology. Dr. Ertan Yilmaz gets special thanks for his support and invaluable friendship. My friends Chris Dever, Dan Mazzucco, Ryan Jones, Ephi Most and Alisa Morss get special thanks for being buddies during the preparation for the all-famous mechanical engineering qualifiers. I would also like to acknowledge the moral support of the goals scored by Fenerbahce striker Pierre VanHooijdonk.

I thank my Mom, Dad, Grand Mom, little brother Tugrul and sister Asli without whose love and support, I would achieve absolutely nothing. I would like to thank my other family members also for their love and caring. I would like to dedicate this

thesis to my grandfather Mehmet Turgaygil, a truly exceptional man who taught me to believe, and to work with belief. May he rest in peace forever.

Contents

List of Figures

Chapter 1

Introduction

This thesis reports a micromechanical label-free biosensor that generates an inherently differential measurement of biomolecular adsorption with respect to a reference surface. This chapter provides a brief introduction to biomolecular sensing and summarizes some currently-used label-based methods, their advantages and disadvantages. Label-free methods are then discussed along with some current techniques, including the particular class of *micromechanical sensors*. The chapter ends with a generic scope of the thesis including chapter summaries.

1.1 Biomolecular detection

The ability to detect biologically significant molecules has tremendous impacts. Disease diagnostics and treatment, drug discovery, understanding cell signaling pathways, and even criminal investigations depend on accurate measurement of biomolecules. There is increasing demand for sensors that can detect biomolecules such as DNA, RNA, and especially proteins with high sensitivity and selectivity both for laboratory use and lab-on-a-chip applications for point-of-care use and portability. The utopic goal of biomolecular detection is to perform fast, sensitive and quantitative profiling of all biomolecules, given a complex mixture. Hence, an ultimate biosensor would have an array of many sensors to detect many molecules at the same time and at high speed. This is also referred to as *high-throughput* biosensing. At present date,

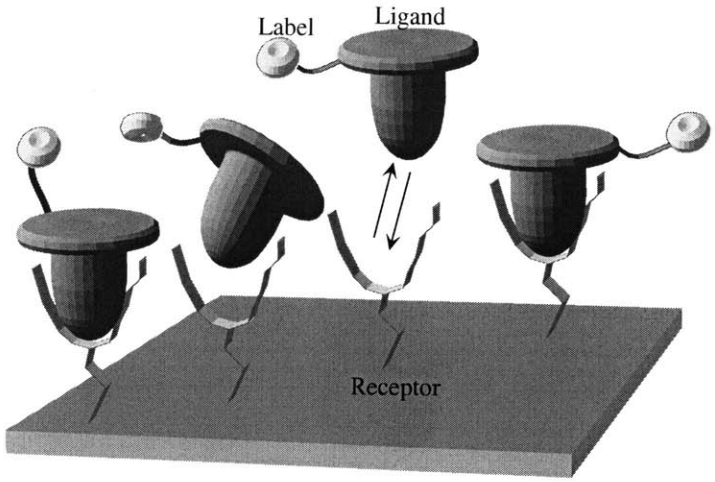

Figure 1-1: Biomolecular detection using labels. Labeled target molecules interact with receptors immobilized on a surface.

the goal is far from complete but significant advances in the field of biosensing are being made that continuously bring the state-of-the-art closer to the goal.

A generic biosensor includes receptor molecules and a signaling mechanism. Receptors are biomolecules that can specifically recognize and bind to target molecules, i.e., ligands that are present in the environment. The signaling mechanism produces a signal representing the receptor-ligand binding. Many current biodetection systems require labels because target molecules do not have intrinsic properties that are useful for direct high-sensitivity detection [1]. Labels are secondary molecules that can reveal signals (eg. optical, radioactive) and are cross-linked to target molecules before performing the detection. Fig. 1-1 illustrates the basic principle of biomolecular detection using labels. Receptor molecules that can bind to specific target molecules are immobilized on a surface. Then, a solution that involves the ligands is introduced onto the surface, and ample time is given for the binding reaction to complete. Finally, the non-binding ligands are washed away, and the surface is imaged. Some common labels are radioactive labels, chemiluminescent labels and fluorescent labels. At present, the most widely used detection system is fluorescence microscopy which uses fluorescent labels. Fluorescence microscopy can perform extremely sensitive measurements. It however has some disadvantages, as discussed below.

Labeling biomolecules is a non-trivial task. First, linking secondary structures to biomolecules introduces the possibility of modifying their original behavior, since most biomolecules have not evolved to act in the presence of additional molecules linked to themselves. Second, depending on the specific target molecule, the labeling process itself can be chemically challenging. This is especially true for proteins. An additional disadvantage of fluorescence microscopy and many other label-based detection methods is that they are designed for end-point-detection, i.e., they are not readily configured to perform real-time detection of binding events. This is because the non-binding targets (which also fluoresce) have to be washed away. Generally, measurements are performed before and after binding, and the results are compared. This is a serious disadvantage because under many circumstances, one may seek information on not only the steady-state of a binding reaction but also its kinetics. Finally, labeling biomolecules involves cost and time. A practical example is *streptavidin.* This commonly used protein is commercially available at a price of $15.90 per 100 μg. It is also possible to purchase streptavidin with the fluorescent label FITC, at a price of $28.95 per 100 μg; almost 100% more expensive than the non-labeled version[1]. Further, the labeling process can take hours to days, which is not desirable for many applications and unacceptable for those that require urgent scanning of a real-life sample in an emergency situation.

Many of these disadvantages can be alleviated by label-free detection methods which avoid disturbances from conjugated labels or handling radioactive materials [2] and also enable real-time detection.

1.2 Label-free biosensing

The absence of the labeling requirement offers the possibility of detection in a broad range of biological systems, since the target molecules no longer need to be processed prior to the detection. Three commonly used and commercialized label-free biosensing methods are ellipsometry, surface plasmon resonance and the quartz crystal microbal-

[1]Sigma Products for Life Science Research, 2003-2004

ance.

Ellipsometry is the first optical technique used for the monitoring of interactions between macromolecules at a surface [3]. It measures the change in polarization state of light reflected from the surface of a sample and yields refractive index and thickness information about the adsorbed layer [2]. Ellipsometry can be used to measure thicknesses down to the size of a single atomic layer.

Surface plasmon resonance (SPR) is an electron charge density wave phenomenon that occurs at the surface of a metallic film under the condition of total internal reflection which forms an evanescent wave that penetrates through the film to its opposite side (the side that accommodates the binding reaction). The evanescent wave is sensitive to the refractive index of the medium on the opposite side of the film and results in an angular intensity dependence of the reflected light beam. Liedberg et al. was the first to demonstrate the use of SPR for biosensing in 1983 [4]. Today, BIACORE is the most popular SPR-based sensor, and can be used to detect receptor-ligand interactions in real-time [5]. SPR measurements are based on refractive index changes and hence cannot differentiate between different molecules of the same group. For example, different proteins have very similar refractive indices, i.e., refractive index change is the same for a given change in concentration [6]. Values for glycoproteins, lipoproteins and even nucleic acids are of the same order of magnitude. SPR thus provides a mass detector which is essentially independent of the nature of the interactants [7].

One disadvantage of both the ellipsometry and the SPR is that they have not yet been scaled (both down in size and up in number). Companies that have commercialized these techniques are investigating possible ways to scale them for high-throughput detection.

Another label-free sensor is the quartz crystal microbalance (QCM). QCM is a mass detector whose operation is based on measuring changes in the resonance frequency of a quartz crystal plate [8]. The crystal is piezoelectric and used in combination with a positive-feedback oscillator circuit to detect its resonance frequency. The resonance frequency of the crystal decreases as particles adsorb onto its surface. The

QCM's basic instrumentation is far less complex and less expensive than the SPR and the ellipsometry. However, operating mechanical resonators in aqueous environments (which is where most biologically significant reactions occur) is challenging due to the effective mass and the damping added by the solution [9]. In addition, QCM is extremely sensitive to temperature changes, hence, the temperature of the fluid in the chamber that accommodates the crystal must be precisely controlled. The most advanced commercialized QCM setup is the *Q-sense* [10] which has a temperature controlled fluidic cell, and a fluid delivery system that is carefully designed to eliminate bubbles. Due to the additional requirements that make QCM operational in solution, the overall system is also not easy to scale for high-throughput detection.

1.3 Microelectronic label-free biosensors

One class of sensors that offers scalability and, hence, the potential for high-throughput detection is microfabricated or MEMS-based biosensors. MEMS technology enables the realization of sensors small enough to be influenced by the presence and/or the quantity of biomolecules, or to be inserted into biologically significant environments such as cells. Small devices in turn enable small packages for portability. Furthermore, microfabrication technology enables building many devices at the same time to form an array of sensors each of which can be used to detect a different molecule simultaneously.

Some earlier versions of microfabricated biosensors operate via the electronic effects induced in them by chemical changes that occur in the surrounding solution. For example, devices that are based on an electrolyte-insulator-semiconductor architecture detect the extent of the depletion region formed in the semiconductor by the change in surface potential that occurs at the electrolyte-insulator interface [11, 12]. Manalis et al. introduced the scanning probe potentiometer (SPP) by integrating a light addressable potentiometric sensor (LAPS with a 100 μm^2 surface area) at the tip of a cantilever [13]. The cantilever structure enabled scanning the sensor through many analytes that remain at distinct locations and hence, the ability to profile pH

changes on the surface of an arbitrary sample [13]. Cooper et al. used the SPP to measure the change in the capacitance of the depletion region in the semiconductor section of the device caused by adsorption of molecules to its insulating surface [14]. Fritz et al. used the SPP to demonstrate the detection of DNA by its intrinsic molecular charge [15].

Microelectronic sensors are inherently scalable, and their instrumentation is relatively simple. They are quite effective in detecting high-charge-density biomolecules in backgrounds with low ionic strength. However, they also have an important disadvantage. Most electronic biosensors detect molecules by their intrinsic charge. There is a specific distance from the surface of the sensor, known as the *Debye length* beyond which, charge posessed by a molecule is shielded or screened by the mobile ions in the solution. Hence, detecting molecules at distances greater than the Debye length, or detecting binding interactions that require high ionic concentration (and hence a short Debye length) is challenging.

Another class of biosensors as discussed below, avoids this problem by detecting mechanical, rather than electronic effects induced by molecular interactions that occur on sensor surface.

1.4 Micromechanical label-free biosensors

It has been shown that intermolecular forces resulting from binding of molecules induce surface stresses [16, 17]. Butt et al. demonstrated that binding-induced surface stress can be detected via the deflection of a micromachined flexible cantilever [18]. Berger et al. used the same technique to measure adsorption of alkanethiols on gold [19]. They coated the top surface of a standard AFM microcantilever with a thin layer of gold, and observed the bending of the cantilever as thiols adsorbed and self-assembled on the gold surface. Berger et al. also showed that bending contribution of the gravimetric effects and the thermal energy released by the chemical reaction that occurs on the surface is negligible, and that the major cause of bending is the surface stress. The preferential binding of target molecules to the two surfaces of

the cantilever that have been prepared to be chemically different results in different surface stresses on the two cantilevers. The difference in the two surface stresses creates a moment that bends the cantilever. The process of chemical preparation of a surface is called *functionalization* of that surface. Functionalization is carried out by exposing one surface of the cantilever to a chemical that is known to bind to (or react with) a specific target.

In recent years, cantilever-based sensors have attracted significant attention and have been used to detect numerous chemical reactions. Researchers demonstrated pH detection by modifying one surface of the cantilever with molecules that react to pH changes in solution [20, 21, 22]. Others detected plastic explosives by coating cantilevers with self-assembled monolayers of mercaptobenzoic acid [23].

In almost all reported experiments, the cantilever dimensions are on the order of 100 μm wide, a few 100 μm long and about 1 μm thick, and the cantilever material is either silicon or silicon nitride. The tip deflection of the cantilever is measured by the *optical lever method* [2], whereby a laser beam is directed at the tip of the cantilever, and the position of its reflection is measured using a position-sensitive photodetector. One surface of the cantilever is usually coated with a thin layer of gold (20-30 nm), usually with a 1-2 nm thick titatium or chromium as an adhesion layer. The gold layer serves to two purposes: 1. to improve the optical reflectivity of the cantilever surface, 2. to allow deposition of thiol-based molecules onto the cantilever surface. The sulphur-gold bond is a strong covalent bond that is often used in functionalization to cross-link molecules to surfaces. Researchers often coat their surfaces with gold, and attach a thiol (-SH) group to one end of their molecules to immobilize them on gold-coated surfaces. This method of surface functionalization is extremely simple and commonly used.

Little is known about the cause and the origin of cantilever bending. It is possible to conveniently *lump* the effects of the surface reaction into a single sensor-independent parameter: *surface stress*. Under some conditions, it is also possible to use surface stress to quantitatively represent a particular reaction. However, studies

[2] To be described in greater detail in Chapter 2.

show that cantilever deflections are very sensitive to surface morphology, order of immobilized molecules, and the funtionalization process [24]. Small variations on the roughness of the surface, or the order and packing of molecules can easily lead to changes in the effective surface stress. A complete model of the bending system requires understanding of the intermolecular forces generated by binding reactions, and the dependence of these forces on the surface properties. Only for the specific case of DNA hybridization were researchers able to qualitatively attribute the nature of cantilever bending to a combination of electrostatic/steric repulsions and configurational entropy assumed by DNA strands before and after hybridization [25]. Unfortunately, a generic model that relates intermolecular forces for a given receptor-ligand reaction to a given set of cantilever surface conditions does not exist, and is beyond the scope of this thesis.

Despite the lack of analytical knowledge of the intermolecular forces, cantilever-based sensors can be designed and used to perform quantitative detection of receptor-ligand reactions, since, the cantilever detects an effective result of the intermolecular forces. Researchers have used cantilevers to detect biologically significant reactions such as DNA hybridization and antigen-antibody interactions [26, 27].

In many of these experiments, researchers used a single cantilever. Using a single cantilever has significant disadvantages. As pointed out earlier, cantilevers are usually coated with a thin layer of gold. The difference in the coefficients of thermal expansion between gold and the cantilever material (silicon or silicon nitride) forms a *bi-material effect* which causes significant amount of bending upon a temperature change. To avoid this problem, reserachers using single cantilevers always controlled the temperature of the fluid that was surrounding the cantilever. Further, a single cantilever is also sensitive to the binding of unwanted molecules to its either surface. This phenomenon is known as *nonspecific binding*. Often, researchers performed sequential control experiments using a different cantilever. However, an ideal control experiment must be performed simultaneously and under the same conditions as the primary experiment to avoid uncertainties introduced by changes in experimental conditions. In experiments using single cantilevers, it is common to observe instabilities,

drifts, and even unexplained changes in drift slope [28].

Fritz et al. of IBM-Zurich used two adjacent micromachined cantilevers to detect DNA hybridization [29]. The gold-coated surfaces of the cantilevers were functionalized with DNA oligonucleotides of different sequences. DNA hybridization on one of the cantilevers and not on the other caused a differential bending, i.e., the bending of one cantilever relative to the other. The differential response was calculated off-line, by subtracting the two signals. The resulting signal was greatly improved, since the effects of temperature changes and long transients resulting from solution injections were significantly reduced. IBM-Zurich group also performed differential detection of multiple DNA sequences by using an array of cantilevers each functionalized with a different DNA sequence [30]. They also detected proteins by functionalizing cantilevers with specific antibodies [31]. Experiments were performed using the optical lever method, whereby, a separate laser beam was focused at the terminus of each cantilever, and the reflected beams were detected separately. Since the method reveals individual signals, the differential response was calculated off-line.

This thesis study reports a micromechanical biosensor that performs an inherently differential measurement. This is achieved by using two adjacent cantilevers that form a sensor-reference pair, and utilizing an interferometric technique to detect the relative deflection between the two cantilevers directly, as opposed to detecting the two responses separately and subtracting them off-line. Hence, the sensor exhibits *mechanical logic* that subtracts the two responses, and reveals a signal that is inherently differential. Interferometric detection also has the advantage of immunity to ambient vibrations which enables detection on a simple laboratory bench without much need for vibration considerations. The optical lever method is very sensitive to ambient vibrations, and its operation requires that the mechanical path between the laser and the photo-detector not sustain any vibrations. In many of the reported experiments, an AFM setup was used, since an AFM setup has a rigid head (the housing for the optical detection elements) and an overall setup that is carefully designed to minimize sensitivity to vibrations.

The thesis presents the design, fabrication and characterization of the interfero-

metric sensor, as well as its application to a receptor-ligand interaction using novel receptors.

1.5 Thesis contents

Chapter 2 covers the design of the differential micromechanical sensor. The underlying mechanisms for cantilever bending are discussed. The optical detection scheme used by the sensor is presented and compared with other optical methods. The chapter ends with a discussion of geometrical considerations that complete the design.

Chapter 3 presents the microfabrication process in detail. The problems encountered during the fabrication and their solutions are also discussed. The results of the fabrication are presented with scanning electron micrographs and optical images.

Chapter 4 describes the characterization of the device. In the beginning of the chapter, the experimental setup is presented. Then, the deflection calibration of the detected optical signal is explained in detail. The dependence of the sensor's response on its geometrical properties is investigated and the sensor's ability to reject nonspecific effects is discussed. Finally, the application of the sensor to a model receptor-ligand system is presented.

Chapter 5 is on the application of the sensor to *aptamers*, an emerging receptor technology. First, a brief intoduction to aptamers is given, and their advantages as receptor molecules are discussed. Then, the application of the sensor to two different aptamer-ligand systems is presented. The experimental results on specificity and selectivity are also discussed. The chapter ends with a verification experiment that was performed using a different sensor.

Chapter 2

Device Design

This chapter describes the design of the micromechanical sensor. First, the mechanisms responsible for cantilever bending are analyzed. The two main causes of bending, namely surface-stress and the bi-material effect are formulated and discussed. In the light of the two major bending mechanisms, the necessity of differential sensing is emphasized. Then, the optical detection scheme is presented, compared with other commonly used ones, and its incorporation into the device is discussed. Finally, geometrical considerations for the differential micromechanical sensor are presented.

2.1 Surface-stress-induced cantilever bending

Cantilever-based sensors have been used by a number of researchers to perform both chemical and biological detection [18, 19, 25, 27, 32, 33]. One cantilever-based method is mass detection by observing the change in the natural frequency of the cantilever. This method, though effective in air and in gaseous media, is rather ineffective in aqueous media because of high damping ratio and effective mass added by the surrounding fluid. Since most biologically significant reactions occur in water or some aqueous media, using cantilevers to perform mass-dependent biological detection is difficult.

In many reported cantilever-based chemical/biological experiments, the measured metric is the static bending of the cantilever which is not caused by a mass change.

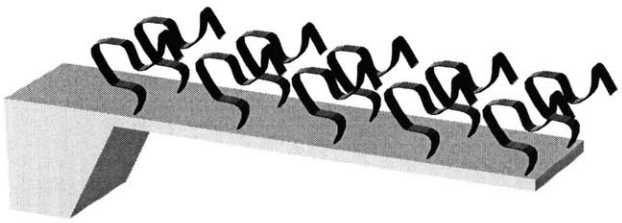

Figure 2-1: Schematic of a functionalized cantilever. Receptor molecules with specific binding affinity for target molecules are immobilized on cantilever's top surface. (Not drawn to scale.)

The static deflection caused by the added mass of biologically or chemically significant molecules would be insignificantly small. As will be demonstrated in a later chapter, it is possible to obtain cantilever bending by changing the pH in the solution. The effect of the pH change is protonation/deprotonation of one surface of the cantilever. The change in mass of the cantilever caused by this effect would be almost infinitesimal. The main mechanism that causes static cantilever bending is an *effective surface stress* generated by the chemical or biological *action layer* which is at least two orders of magnitude thinner than the cantilever itself. The action layer is present only on one of the cantilever's surfaces, and is generally formed *a priori* by depositing receptor or probe molecules (that can recognize specific target molecules) on a particular surface, or by chemically modifying that surface to make it sensitive to a specific chemical reaction. This process is called *functionalization* of the surface.

Fig. 2-1 illustrates a cantilever with its top surface functionalized. During a reaction, the functionalized surface becomes chemically modified and generates a surface stress. The modification can be either a change in the conformation of the functionalized molecules, or binding of target molecules to the functionalized surface, or a combination of both. The nature and the magnitude of the interactions that occur between the individual molecules on the cantilever surface are not completely understood. Only for the specific case of DNA hybridization were researchers able to discuss a few mechanisms that may possibly cause cantilever bending. These involve

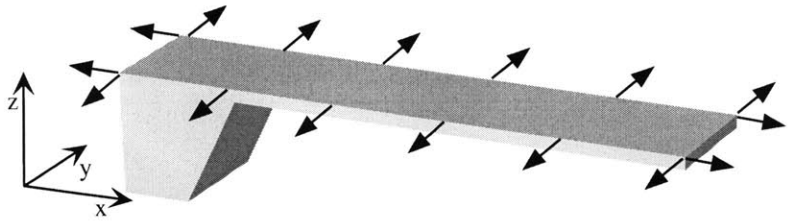

Figure 2-2: Effective surface stress that represents the mechanical equivalent of biomolecular interactions that occur on cantilever's top surface.

steric and/or electrostatic repulsion, and entropic forces that result from changes in the molecules' willingness to occupy a certain space [25], and hydration forces [24]. However, there is no generic mathematical formulation to predict the intermolecular forces between immobilized molecules in the presence of a given target molecule or a chemical environment. Fortunately, the lack of knowledge of intermolecular forces does not prevent one from developing a device that can produce a signal representing a result of those forces, as long as one can *lump* all of the interactions that occur on the surface into a single parameter that is independent of the device's mechanical or geometrical properties. This is accomplished by replacing the presence and the effect of the *action layer* by an *effective surface stress* as shown in Fig. 2-2. The dependence of cantilever motion on the surface stress and the mechanical and the geometrical properties of the cantilever is analyzed below.

The elasticity relations of basic plate bending in two dimensions are

$$\epsilon_x = \frac{\sigma_x - \nu\sigma_y}{E} \tag{2.1}$$

$$\epsilon_y = \frac{\sigma_y - \nu\sigma_x}{E}. \tag{2.2}$$

At the same time,

$$\epsilon_x = -\frac{z}{\rho_x} \tag{2.3}$$

$$\epsilon_y = -\frac{z}{\rho_y}. \tag{2.4}$$

In the above equations, ϵ, σ and ρ represent strain, stress and the radius of curvature respectively. E and ν stand for the Young's modulus and the Poisson's ratio of the cantilever material respectively. Equating the corresponding strain relations gives

$$\sigma_x = -\frac{Ez}{\rho_x} + \nu\sigma_y \tag{2.5}$$

$$\sigma_y = -\frac{Ez}{\rho_y} + \nu\sigma_x. \tag{2.6}$$

Substituting 2.6 into 2.5, and 2.5 into 2.6 respectively gives

$$\sigma_x = -\frac{Ez}{1-\nu^2}\left(\frac{1}{\rho_x} + \frac{\nu}{\rho_y}\right) \tag{2.7}$$

$$\sigma_y = -\frac{Ez}{1-\nu^2}\left(\frac{1}{\rho_y} + \frac{\nu}{\rho_x}\right). \tag{2.8}$$

Bending moments associated with the stresses are expressed as

$$M_y = \int_{-\frac{t}{2}}^{\frac{t}{2}} \sigma_x w z dz \tag{2.9}$$

$$M_x = \int_{-\frac{t}{2}}^{\frac{t}{2}} \sigma_y w z dz. \tag{2.10}$$

Substituting 2.7 into 2.9, and 2.8 into 2.10 gives

$$M_y = -\frac{wt^3}{12}\frac{E}{1-\nu^2}\left(\frac{1}{\rho_x} + \frac{\nu}{\rho_y}\right) \tag{2.11}$$

$$M_x = -\frac{wt^3}{12}\frac{E}{1-\nu^2}\left(\frac{1}{\rho_y} + \frac{\nu}{\rho_x}\right). \tag{2.12}$$

Now, *surface stress* is defined as the integral of the normal stress σ_m in the monolayer over its thickness:

$$N = \int_0^{t_m} \sigma_m dz. \tag{2.13}$$

N is the surface stress acting on the top surface of the cantilever, and has the unit N/m (as opposed to N/m^2 which is the unit of normal stress). N can be modeled as *force per unit length* acting along the edges of the top surface of the cantilever (Fig.

2-2). Hence, the total force acting along each side of the top surface of the cantilever is NL, and similarly, that along the back and front edges is Nw. Accordingly, the effective moments that are caused by the surface stress N are

$$M_x = NL\frac{t}{2} \tag{2.14}$$

$$M_y = Nw\frac{t}{2}. \tag{2.15}$$

Equating 2.11 to 2.15, and 2.12 to 2.14 reveals that

$$\frac{1}{\rho_x} = \frac{1}{\rho_y} \tag{2.16}$$

which simplifies the analysis. Substituting 2.16 into 2.11, equating the result with 2.15 and solving for curvature gives

$$\frac{1}{\rho_x} = -\frac{6}{t^2}\frac{1-\nu}{E}N. \tag{2.17}$$

For small out-of-plane deflections z along the cantilever's main axis x,

$$\frac{1}{\rho_x} \simeq \frac{d^2z}{dx^2} \tag{2.18}$$

which is solved trivially and combined with 2.17 to yield a tip deflection of

$$\delta = -3\frac{1-\nu}{E}\frac{L^2}{t^2}N. \tag{2.19}$$

Eq. 2.19 is the *Stoney's equation* [34]. Until now, the surface stress was represented by N to prevent confusion with other stress expressions used in the derivation. At this point, N is replaced with σ for consistency with the literature that cite Stoney's equation [19, 25, 27, 35]:

$$\delta = -3\frac{1-\nu}{E}\frac{L^2}{t^2}\sigma. \tag{2.20}$$

Eq. 2.20 implies that, given a cantilever deflection value, one can represent a chemical/biological event on the cantilever surface with a single independent parameter,

σ, with the units N/m . Accordingly, one can perform a series of different biological experiments and represent each one with a particular σ value.

Strictly speaking, it is not possible to represent a surface reaction with a single parameter calculated using a deflection value and the cantilever's mechanical and geometrical properties. Cantilever deflections are very sensitive to the morphology of the surface. Hence, characterization and control of nanoscale self-assembly processes that determine the probe molecule immobilization, i.e., surface functionalization is imperative for reliable design [24]. Unfortunately, the behavior of immobilized molecules on the cantilever surface and how they interact with each other under a given set of environmental conditions is not completely understood. Further, biological systems are not necessarily time-independent, i.e., a group of self assembled probe molecules may undergo conformational modifications over time, which may in turn influence the way they react with target molecules. Nevertheless, there is no evidence to suggest the existence of first-order dependence of a surface reaction on the mechanical or the geometrical properties of the cantilever. As will be demonstrated in the device characterization chapter, and also in light of the literature [27], Eq. 2.20 is a surprisingly good approximation.

2.2 Temperature-induced cantilever bending

Cantilever-based sensors are generally coated with a thin layer of gold on one side. The thickness of the layer is about 20-30 nm and does not significantly influence the mechanics of the cantilever. The gold layer serves to two purposes: 1) To enable thiol-based functionalization. The sulphur-gold bond is covalent and quite strong. Once receptor molecules are thiolated, i.e., modified to include a sulphur group at one end, it is simple to expose them to a gold surface and form a self-assembled monolayer (SAM). 2) To improve optical reflectivity. As will be discussed in the next section, most cantilever-based techniques utilize optical methods to detect the cantilever deflection.

There is a disadvantage of using a gold layer. The cantilever material is usually

silicon or silicon nitride. Depositing a metal layer on one surface of the cantilever forms a *bi-material effect* due to the difference in the thermal expansion coefficients of the cantilever material and the metal. The bi-material effect can result in significant cantilever bending upon changes in temperature [36]. Depending on its magnitude, bending caused by a temperature change may not be differentiated from that caused by a chemical/biological reaction. Hence, this particular mechanism is worthy of a separate analysis.

The model to be used for the analysis can remain the same as shown in Fig. 2-1, except the action layer is replaced with a gold layer of thickness t_g and Young's modulus E_g. Two dimensional elasticity relations for a plate that experiences a temperature change are

$$\epsilon_x = \frac{\sigma_x - \nu\sigma_y}{E} + \alpha\Delta T \tag{2.21}$$

$$\epsilon_y = \frac{\sigma_y - \nu\sigma_x}{E} + \alpha\Delta T. \tag{2.22}$$

At this point, Poisson effects are ignored for simplicity and hence, the structure is modeled as a simple beam. Given the fact that the structure is a cantilever with a length about 5 times its width [29], one would expect the maximum deflection to occur at its tip. Hence, to a first-order approximation, ignoring Poisson effects should not lead to a significant error. Rearranging the strain-curvature relation (Eq. 2.3) reveals

$$\sigma_x = -E\Big(\frac{z}{\rho_x} + \alpha\Delta T\Big). \tag{2.23}$$

The moment formed by the stress in the beam's cross-section is

$$M_y = \int_{-a}^{t-a+t_g} \sigma_x w z dz. \tag{2.24}$$

Here, a is the distance of the neutral axis from the bottom surface of the cantilever[1]:

$$a = \frac{Et^2 + 2E_g t t_g + E_g t_g^2}{2Et + 2E_g t_g}. \tag{2.25}$$

[1]Since the cantilever is made of two layers, its neutral axis is not simply $\frac{t}{2}$.

Substituting 2.23 into 2.24 and realizing that for static equilibrium moment must be zero (no external moment applied) yields

$$\frac{Ew}{3\rho_x}\Big((t-a)^3+a^3\Big)+\frac{Ew\alpha\Delta T}{2}\Big((t-a)^2-a^2\Big)+$$
$$+\frac{E_g w}{3\rho x}\Big((t-a+t_g)^3-(t-a)^3\Big)+\frac{E_g\alpha_g\Delta T w}{2}\Big((t-a+t_g)^2-(t-a)^2\Big)=0 \quad (2.26)$$

Rearranging and solving for curvature gives

$$\frac{1}{\rho_x}=\frac{-6(\alpha_g-\alpha)(t+t_g)\Delta T}{t^2\left(4+6\frac{t_g}{t}+4\frac{t_g^2}{t^2}+\frac{E_g}{E}\frac{t_g^3}{t^3}+\frac{E}{E_g}\frac{t}{t_g}\right)}. \quad (2.27)$$

Integrating twice along the length of the cantilever yields the tip deflection:

$$\delta=\frac{-3(\alpha_g-\alpha)(t+t_g)L^2}{t^2\left(4+6\frac{t_g}{t}+4\frac{t_g^2}{t^2}+\frac{E_g}{E}\frac{t_g^3}{t^3}+\frac{E}{E_g}\frac{t}{t_g}\right)}\Delta T. \quad (2.28)$$

Eq. 2.28 can be further simplified for the case of small gold thickness:

$$\lim_{\frac{t_g}{t}\to 0}\delta=-3(\alpha_g-\alpha)t_g\frac{E_g}{E}\frac{L^2}{t^2}\Delta T. \quad (2.29)$$

Fig. 2-3 shows the temperature-dependence of cantilever bending as a function of gold thickness. The plot shows an overlay of both the full model (Eq. 2.28) and the approximation for thin gold layer (Eq. 2.29) for a silicon nitride cantilever with 500 μm length, 100 μm width, and 1 μm thickness (typical cantilever dimensions). The full model states that temperature sensitivity increases with gold thickness for relatively thin gold layers, but eventually reaches a peak and starts to descend. This behavior makes intuitive sense. When the gold thickness is relatively small, it does not influence the cantilever bending stiffness but contributes to the bi-material effect. As the gold thickness increases, its contribution to bending stiffness increases and, after a certain point, overwhelms the bi-material effect. The thin gold layer approximation, as expected, deviates significantly from the full model as gold thickness increases.

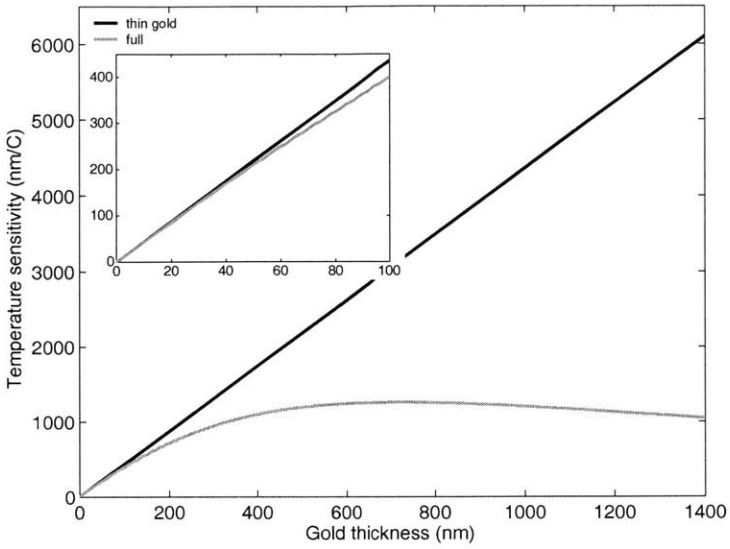

Figure 2-3: Temperature-induced bi-material cantilever bending. Both the full model and the thin gold approximation are shown.

For purposes of optical reflectivity and thiol-based chemical functionalization, a gold thickness of about 20 nm suffices. For gold thicknesses around this range, Fig. 2-3 shows that Eq. 2.29 (the thin gold layer model) is quite accurate.

It is interesting to see that the thin gold layer approximation and the Stoney's equation have the same geometrical dependences. This suggests that bi-material effect can be represented as an effective surface stress. It also implies that one cannot differentiate between surface-stress-induced bending and temperature-induced bending. Based on available references, a typical bending caused by a biological interaction is about 10 nm [29] for a cantilever with dimensions similar to those assumed to form Fig. 2-3. According to 2.29, this much bending can be caused by a temperature change of only 0.12 °C, assuming 20 nm gold thickness. Hence for reliable detection, it is essential to significantly reduce the effects of temperature change.

In biological/chemical detection experiments reported in the literature that involve using a single cantilever, the temperature of the solution that surrounds the cantilever was precisely controlled. One of the main design goals of this thesis study is to eliminate the need for such robust temperature control.

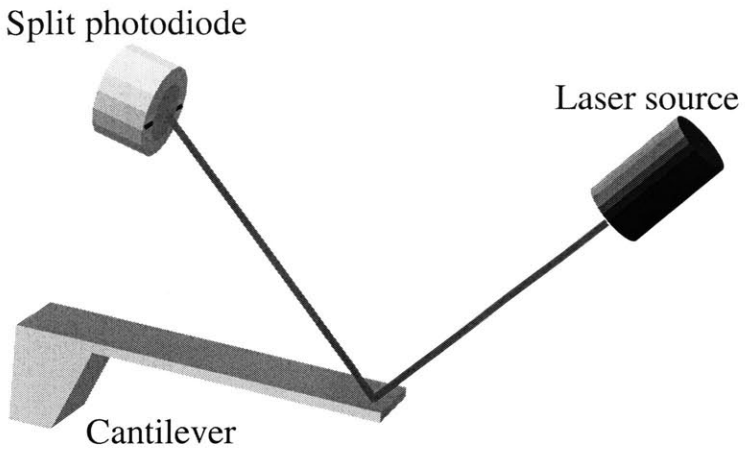

Figure 2-4: Optical lever method. A laser beam is reflected from the tip of the cantilever; its location is detected using a split photodiode.

2.3 Optical detection

2.3.1 Optical lever method

Deflections caused by biological interactions are nanoscale and require a sensitive detection scheme. One method that offers extremely sensitive motion detection is tunneling. However, for stability purposes, tunneling systems need to be operated in a feedback mode which requires non-trivial circuitry and electrical configuration. Furthermore, operating a tunneling system in aqueous media is extremely difficult due to leakage currents [37]. Optical methods are relatively simple and require minimal electrical configuration. One optical method that is sensitive, relatively simple, and widely used is the *optical lever method.*

Fig. 2-4 illustrates the basic principle of the optical lever method. A laser beam is focused at the tip of the cantilever and the location of the reflected beam is measured using a split photodiode. The output of the photodiode is then converted to volts, amplified and sent to a data acquisition interface. This method is relatively simple, i.e., does not require any circuitry or any fabrication-level manipulation of the cantilever chip. Also, once a cantilever chip is enclosed in a chamber, the only

requirement is a transparent opening at the top of the chamber to allow the passage of the laser beam.

The optical lever method is very popular and is used by almost every atomic force microscope (AFM) system. The main difficulty associated with this method is its sensitivity to laser pointing noise and mechanical vibrations. The optical lever method cannot distinguish the laser pointing noise from the cantilever motion since both will result in a signal that will be detected by the photodetector. Mechanical system noise such as the jittering of the laser source or vibration of the photodetector has the same effect. Studies show that most of the total noise in a basic optical lever system (one that is similar to that on Fig. 2-4) is constituted by a combination of pointing noise and mechanical vibrations [38]. Hence, for reliable operation of the optical lever method, the mechanical path between the laser source and the photodiode must undergo minimum vibration. This can be achieved by minimizing the compliance of the mechanical path between the laser source and the photodetector. Researchers who used the optical lever method used a setup that minimizes mechanical vibrations (typically an AFM setup which has a very rigid head that houses the laser source and the photodiode).

As described below, there is another optical detection scheme that is inherently insensitive to vibrational movements of the laser and the photodetector as well as the laser pointing noise. Such a scheme is directly operable on a simple laboratory bench.

2.3.2 Interferometry method

One optical detection method that is immune to laser pointing noise and vibration of the optical components is interferometry by interdigitated (ID) fingers. This method relies on an intensity measurement of an optical signal, rather than a position measurement. Fig. 2-5 shows the operation principle of this method. The two sets of ID fingers form a phase sensitive diffraction grating. When illuminated by a coherent optical beam, the grating reflects the beam into several modes. The intensity of each mode depends on the displacement between the two finger sets. For example the

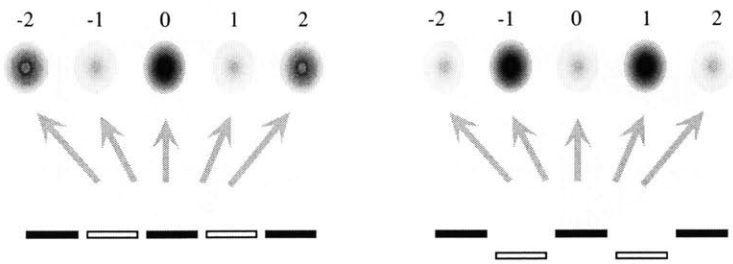

Figure 2-5: Operation principle of interferometric deflection detection using interdigitated(ID) fingers. Diffraction modes change in intensity as ID finger sets move relative to each other.

intensity of the 0^{th} order diffraction mode is given by

$$I_0 \propto cos^2\Big(\frac{2\pi}{\lambda}\xi\Big) \tag{2.30}$$

and the intensity of the 1^{st} order mode is given by

$$I_1 \propto sin^2\Big(\frac{2\pi}{\lambda}\xi\Big) \tag{2.31}$$

where λ is the illumination wavelength and ξ is the relative displacement between the two ID finger sets [38]. Equations 2.30 and 2.31 assume that the ID fingers of each set are perfectly co-planar, hence the distance between the two sets is represented by a single parameter, ξ. Equations 2.30 and 2.31 imply that odd and even modes are out of phase. When the two ID finger sets are perfectly co-planar, i.e. $\xi = 0$, even modes have maximum intensity while odd ones are dim. As ξ increases, even modes get dimmer, whereas odd modes get brighter. When $\xi = \frac{\lambda}{4}$, the initial brightness pattern is completely reversed; even modes are dim, and odd modes are bright. This is also illustrated by Fig. 2-6 in which Eqs. 2.30 and 2.31 are co-plotted with unity amplitude. The intensity of only one mode is needed to detect the displacement of one finger set with respect to the other. Since the relationship between the modal intensity and the displacement is known analytically, calibration can be performed by

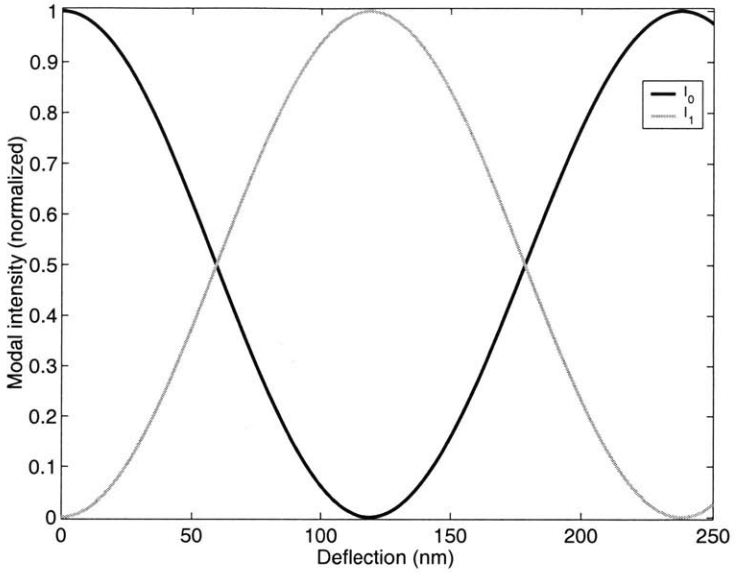

Figure 2-6: Variation of 0^{th} and 1^{st} modal intensities with relative distance between the ID finger sets.

using either 2.30 or 2.31 depending on which mode is chosen for detection. Manalis et al. introduced the use of ID fingers for atomic for microscopy and showed that sub-angstrom level resolution can be achieved in spite of the significantly relaxed alignment tolerances [39].

Analysis and design of ID fingers for displacement sensing was undertaken in detail by Yaralioglu et al. and Minne et al. [38, 40]. Accordingly, some care must be used while designing the geometry of the ID fingers, but otherwise the performance of the interferometer is not notoriously dependent on small design errors. The first rule of thumb is that the number of finger pairs must be greater than 4. This is necessary for separation of modes, i.e., for preventing them from overlapping with each other. Second, the finger width must be larger than finger spacing. This ensures that most of the optical energy is reflected from the fingers (as opposed to passing through the gaps between them) and also that the reflected optical energy gets distributed mostly over the low-order modes i.e., 0^{th}, 1^{st} and 2^{nd}. This is desirable because only one mode is needed for detection, and it is advantageous to concentrate the optical energy to as few modes as possible to ensure and increase visibility during alignment.

It is unnecessary to waste the optical energy over many modes despite the fact that only one of them will be needed. Finally, the overall surface area of the grating must be about the size of the laser beam's spot. A typical diameter (or main chord) of a laser diode beam's cross-section is on the order of 100 μm, and can be made as small as 30 μm by focusing the beam with a lens.

Accordingly, a grating with 6 ID finger pairs (12 fingers total), 4 μm finger width, and 2 μm finger spacing should provide good spatial separation of diffraction modes, and ensure that low-order modes possess more optical energy than the high-order ones. In combination with the above dimensions, a finger length of about 50 μm should provide a sufficient surface area for a laser beam of typical size. As will be demonstrated in the device characterization chapter, the designed interferometer is only limited by the sub-angstrom-level thermomechanical noise of the cantilever to which the interferometer is attached (except for the $1/f$-type low frequency noise region (less than 40 Hz)). The next section discusses the integration of interferometry with a cantilever-based micro-structure to form a mechanical sensor that generates an inherently differential readout.

2.4 Integration of optical and mechanical subsystems

2.4.1 Differential detection

It was discussed earlier that a bi-material microcantilever is very sensitive to ambient temperature changes, and that researchers who used a single cantilever to perform biomolecular detection had to use temperature control units to increase the reliability of their measurements. However, temperature sensitivity of the cantilever is not the only problem with using a single cantilever for biological or chemical measurements.

The target molecule, before being injected into the fluidic cell that accommodates the cantilever, is often dissolved in a buffer solution that allows binding of that target molecule with the particular receptor molecule immobilized on the can-

tilever. The buffer solution, depending on the particular target-receptor interaction may involve many other molecules that are necessary either to stabilize the activity of the target molecule (a specific pH, ionic strength etc.) or to provide a physiologically stable background. How these molecules interact with either cantilever surface (functionalized or free) is difficult to predict. These molecules in combination with other unwanted molecules and contaminants can easily bind nonspecifically to either cantilever surface and corrupt the measurement.

Furthermore, control experiments must be performed using a separate cantilever that is functionalized with a molecule that is not expected to interact with the target molecule. Researchers often use a cantilever different from the one used for the specific binding experiment, perform a separate functionalization process, place the die in the fluidic cell, perform a new optical alignment process, and repeat the experiment. An ideal control experiment must occur at the same time, and under exactly the same conditions as the main receptor-ligand binding experiment. Sequential (as opposed to simultaneous) control experiments introduce many uncertainties about validity and reliability.

One way to eliminate the need for a temperature control unit, significantly reduce the effect of nonspecific binding and improve the reliability of the control experiment is to perform differential detection, i.e., to perform a simultaneous detection relative to a control surface. This does not remove all uncertainties described above, since two surfaces can never be completely identical, but it reduces the uncertainties significantly.

Fritz et al. used the optical lever method to perform differential detection of DNA hybridization [29]. They simultaneously detected the deflections of two adjacent microfabricated cantilevers; one functionalized with a specific sequence, the other with a random sequence. Then, they subtracted the two responses off-line to obtain the differential response. The individual signals retrieved from cantilevers were almost unintelligible. But the differential signal indicated a clear bending caused by hybridization of a DNA strand with a sequence that is complementary to that of the specific strand immobilized on one of the cantilevers.

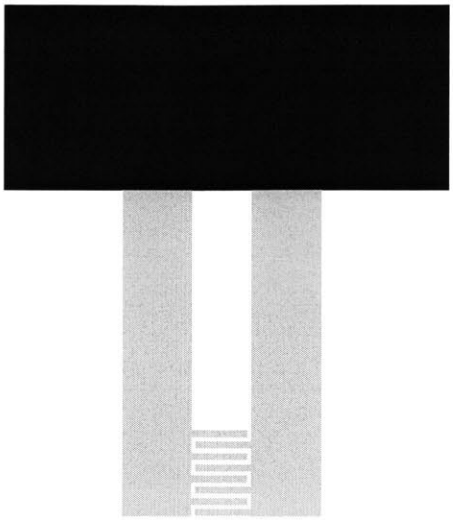

Figure 2-7: Differential interferometric sensor: two adjacent cantilevers with ID fingers in between.

2.4.2 Inherently differential optical-mechanical sensor

The study of Fritz et al. was performed using the optical lever method, whereby, the deflection of each cantilever was measured separately. The main goal and contribution of this thesis study is a biosensor that generates a single signal that is inherently differential. This can be achieved by the ID interferometer. From Fig. 2-5, it is possible to visualize the use of ID-based interferometry to perform differential detection: by placing the interferometer between two adjacent cantilevers. Accordingly, one of the ID finger sets can be attached to the tip area of one cantilever (sensor), and the other ID set can be linked to that of the other cantilever (reference). Since the intensity of a diffraction mode reflected from the grating represents the relative distance between the two ID finger sets, it also automatically represents the distance between the tips of the two cantilevers.

One may immediately envision two adjacent cantilevers that extend from a silicon die (in the same configuration as two adjacent diving boards), with an ID interferometer between their tip areas. This is illustrated in Fig. 2-7. Intuitive and convenient as this concept is, it has a significant practical problem. Before the experiment, each cantilever must be functionalized separately with different chemicals (to accommo-

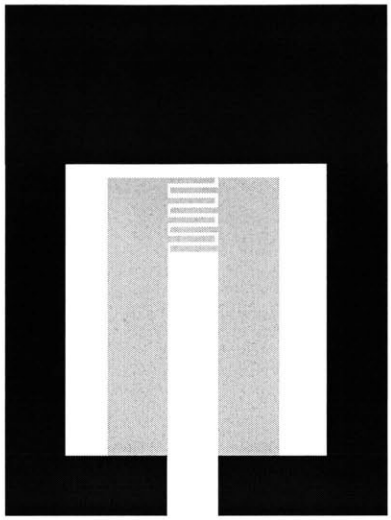

Figure 2-8: Differential interferometric sensor that allows functionalization: reversed cantilever orientation.

date different immobilized molecules). The easiest method for accomplishing this is to insert each cantilever into a micropipette that accommodates the fluid in which the receptor molecules are dissolved. The concept that is illustrated in Fig. 2-7 does not enable this, due to the fact that the ID structure between the tip areas of the two cantilevers prevents separate insertion of each cantilever into a micropipette. It is not an option to re-locate the ID structure further back towards the base of the cantilevers, since the deflection is minimum close to the base.

It is necessary to modify the concept to allow individual insertion into a pipette, without compromising the effectiveness of the ID interferometer. This can be achieved by reversing the orientation of the cantilevers, i.e., by making the cantilever tips point towards the die. This concept is illustrated in Fig. 2-8. The cantilevers (grey in color) are relatively thin. Their bases are the intersections of grey and black colors, and their tips are closer to the die. The black sections constitute relatively thick, and rigid supports for the cantilevers and connect them to the die (also black). This concept allows functionalization by insertion of each cantilever separately into a micropipette, without compromising the ID structure.

The main challenge of the concept in Fig. 2-8 is the fabrication of the supports.

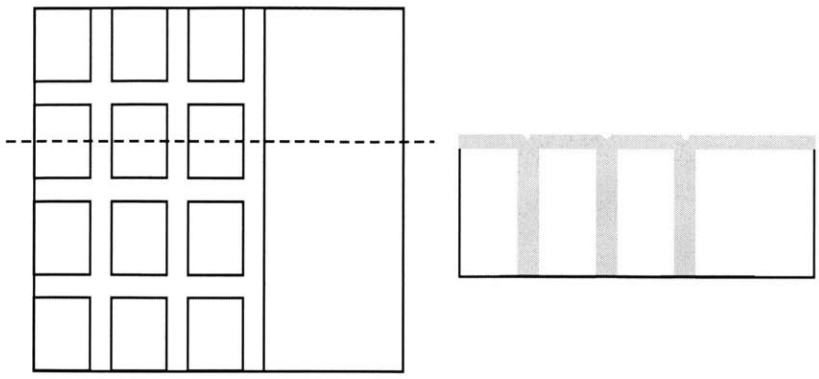

Figure 2-9: Cantilever support concept: Trench pattern etched into wafer (top-view) and the resulting cross-section following thin film deposition.

They have to be thicker than the cantilevers, which mandates a step change in the thickness of the structural cross-section (the intersection of the grey and the dark sections). At the same time, these supports cannot be as thick as the die (about 0.5 mm for a standard 4 inch silicon wafer). In that case, the supports and the die would form an enclosure, and the overall structure would become a potential bubble trap. Given the fact that the structure will be immersed in an aqueous environment, it is imperative to be cautious with bubbles. Any bubbles trapped underneath the cantilevers would hamper their motion, and/or interfere with the operation of the optical detection system. Although a separate chapter is devoted to the details of microfabrication, a few issues will be addressed here, since they influence the design significantly.

It would be simple to fabricate the device shown in Fig. 2-8 by deep-reactive-ion-etch(DRIE)-based bulk micromachining of a silicon-on-insulator (SOI) wafer. However, it would be difficult to form a step-change in thickness at the cantilever base/support intersection, unless one is willing to have the supports as thick as the die. As described, this is undesirable due to potential bubble trapping. This can be alleviated by using surface micromachining techniques and fabricating the structure from a thin film deposited onto a silicon wafer. The support structure can be formed by making the thin film conform to a trench structure that is first etched into the silicon wafer. Fig. 2-9 shows the top view of a wafer with trenches to be filled by thin

film deposition, and the cross-section of the resulting structure after the completion of the deposition. Trenches are etched into the silicon wafer and filled conformally by depositing a thin film. The structure can then be released with a chemical that etches the bulk silicon but not the thin film. As a result, the part of the structure that is formed by filling the trenches has a larger bending stiffness. For the current application, this can be used as a support for the part that is formed by the film deposited on the trenchless and flat area of the silicon wafer, which can be patterned to form the cantilever(s). The thickness of the support structure, and hence the size of the step-change in cross-sectional thickness is directly controlled by the depth of the trench etched into the wafer. The width of the trench on the other hand depends on the film thickness and should be twice the film thickness to ensure the filling of the trench. Complete filling of the trench is desirable to prevent problems of photoresist coverage that might occur during photolithography steps. As shown in Fig. 2-9, small indentations are expected at the intersection of the trenches, but making the trench width twice the film thickness should minimize this effect. This simple technique can also be used in future studies that require fabrication of structures with varying cross-sections.

Fig. 2-10 shows the finalized concept, which is the integration of the interferometric differential sensor with the developed technique of fabricating varying cross-sections. The supports are thicker than the cantilevers and have a grid structure which is formed simultaneously with the cantilevers. One surface of the device is coated with a thin layer of gold. The ID fingers between the cantilevers enable direct detection of differential bending. There are also ID fingers between each cantilever and its support. These enable detecting the absolute bending of each cantilever. The reference cantilever can be actuated with a secondary laser source to bias the interferometer at its most sensitive point. The actuation laser can be simply aligned to heat the base of the reference cantilever and cause it to bend due to the bi-material effect.

A common material that is used to fabricate cantilever structures is silicon-rich silicon nitride. This film can be deposited with a 10:1 ratio for DCS:NH_3 gases.

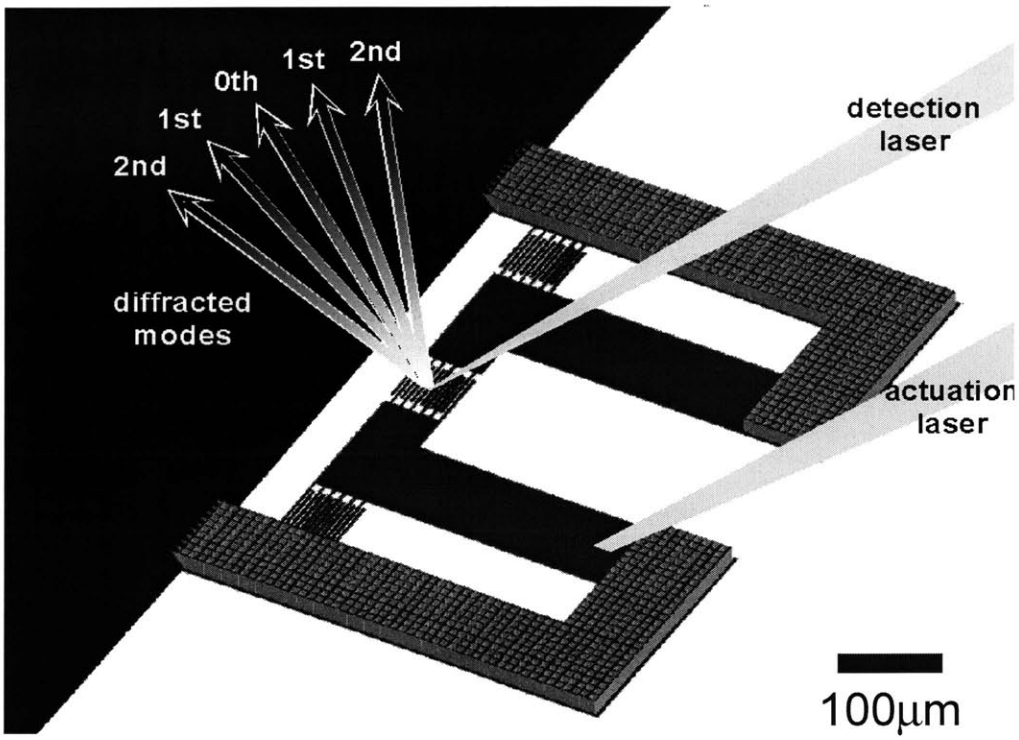

Figure 2-10: Differential micromechanical sensor concept.

This causes low stress in the film and minimizes bending of the cantilevers upon being released from the silicon wafer's surface. Many commercially available AFM cantilevers are made from low-stress silicon nitride mainly to prevent bending upon release and produce cantilevers that are as flat as possible. Low-stress silicon nitride is also suitable for the fabrication of the current design. It can be deposited on a silicon wafer to form the cantilevers and also the supports, and can be released with a KOH solution, since KOH etches silicon but not silicon nitride.

An appropriate set of dimensions for the cantilevers are 1 μm thickness, 100 μm width and 500 μm length. These dimensions are *appropriate* but not necessarily *optimal*. Unfortunately, an analytical model that fully explains the relationship between intermolecular surface forces and geometrical properties of the cantilever is not present and is beyond the scope of this thesis. Hence, it is difficult to mathematically pinpoint the dimensions for optimal operation of the cantilevers in a chemical/biological environment. However, dimensions that are plausible from the sensitivity and res-

olution point-of-view can be selected in light of the Stoney's formulation and the thermomechanical cantilever noise. Combining sensitivity-based plausibility arguments with those based on fabrication limitations, basic mechanical concerns, and also predictions based on literature yields the above set of appropriate dimensions.

The thickness of the cantilever and the width of the trenches (formed to define the support structure) are related. 1 μm film thickness implies 2 μm width for trenches. 2 μm feature size is achievable but is close to the limits of standard photolithography. Hence, thicknesses less than 1 μm are not desirable.[2] According to Stoney's equation (Eq. 2.20), stress-induced cantilever bending has no width dependence (neither does temperature-induced bi-material bending). However, the dependence of the self assembly of receptor molecules during functionalization on the total surface area is not known. Larger width would result in a larger surface area, and a greater total number of receptor molecules. However, first, it is not known whether a greater number of molecules would always result in a more optimal surface. Second, too large a width would increase warping effects near the tip of the cantilever which would kink the ID fingers and result in a signal that would be perceived as cantilever deflection. 100 μm width is on the same order with the widths of commercially available cantilevers and those that are reported in the literature.

Length is the remaining geometrical parameter, and can be chosen via the Stoney's equation. According to literature, surface stress generated in a typical biological receptor-ligand binding interaction is on the order of 0.01 N/m. Fritz et al. report a surface stress value of 0.005 N/m for DNA hybridization [29]. This surface stress corresponds to 16 nm of tip deflection for a silicon-rich silicon nitride cantilever with material properties [36] $E = 180$ GPa and $\nu = 0.27$ and geometrical properties $L = 500\ \mu m$ and $t = 1\ \mu m$. A finite element analysis[3] performed on such a cantilever excited by 0.005 N/m of *force per unit length* (applied along the edges of its top surface) also yields 16 nm of tip deflection. This deflection value is about that reported by Fritz et al. (10 nm).

[2]The author managed to fabricate 0.5 μm-thick devices (1 μm trench width) with extreme caution during photolithography of trenches.

[3]ProEngineer was used for drawing an simulation.

According to Stoney's equation alone, one must maximize the parameter L^2/t^2 for maximum deflection sensitivity to a given surface stress. This however will reduce both the spring stiffness and the natural frequency of the cantilever which will significantly increase the thermomechanical noise level of the cantilever [41]:

$$\delta = \sqrt{\frac{4K_bT}{QK\omega_n}}. \tag{2.32}$$

Here, Q, K, and ω_n represent the quality factor, stiffness, and the fundamental natural frequency of the cantilever respectively. K_b, and T stand for the Boltzmann constant and room temperature respectively. The formulae for the spring stiffness and the natural frequency [42] of the cantilever are respectively:

$$K = \frac{1}{4}Ew\frac{t^3}{L^3} \tag{2.33}$$

$$\omega_n = 1.0161\sqrt{\frac{E}{\rho}}\frac{t}{L^2}. \tag{2.34}$$

Substituting 2.33 and 2.34 into 2.32 reveals that thermomechanical noise is scaled by $L^{2.5}/t^2$. Hence, increase in Stoney sensitivity results in higher thermomechanical noise which is random in nature and will not be taken out by differential detection. Furthermore, decreasing the natural frequency alone increases the cantilever's susceptibility to ambient vibrations (assuming that the base of the cantilever is excited). In addition, longer and thinner cantilevers are more likely to cause stiction problems during a wet release.

The above dimensions and material properties (with ρ = 3400 kg/m^3 [43]) yield K = 0.036 N/m and $\omega_n = (2\pi)4707$ rad/s, and for Q = 10, a thermomechanical noise level of 0.01 Å/$\sqrt{Hz}$ (Eq. 2.32). This corresponds to an RMS deflection value of 0.4 Å over a 1000 Hz bandwidth (which is much larger than that of a typical biological reaction that occurs over 10 minutes). This noise level is far less than the expected cantilever deflection caused by a typical DNA hybridization event (16 nm as mentioned before). The above Q is plausible for a microcantilever (with above

properties) that vibrates in air [4]. When surrounded by fluid (during a biological experiment), Q will decrease significantly due to the added viscosity of the fluid. For a typical Q value of 1 [44], the resulting thermomechanical noise level increases to 1.2 $Å_{RMS}$ which is still much less than the expected experimental deflection values. Subsequently, if the resolution of the system is dictated by the thermomechanical noise of the cantilever, the resulting signal-to-noise ratio should be on the order of 100.

However, at frequencies of interest (time scales greater than 1 minute), thermomechanical noise is no longer the limiting factor, and the resolution is limited by the $1/f$ type low-frequency noise that is on the order of 1 nm [29]. Typical sources of this type of noise will be discussed further in Chapter 4. Unfortunately, an analytical expression that relates the low-frequency behavior of a chemically functionalized microcantilever in solution to its geometric and material properties is not available. Hence at this point, the resolution of the system will simply be assumed as 1 nm.[5] In spite of this relatively high noise level, the expected signal is still at least an order of magnitude larger. Consequently, the length (in combination with the rest of the chosen geometrical parameters) and the material are expected to generate a well detectable signal upon application of a surface stress that is typical for a biomolecular interaction.

For the purpose of confirming the validity of Stoney's equation, the geometrical parameters were varied on the mask, and devices with various lengths (500 μm and 350 μm) and thicknesses (1 μm and 0.5 μm) were fabricated.

To minimize the effect of warping near the tips of the cantilevers, the areas in the vicinity of the ID fingers were stiffened by the grid structure. Fig. 2-11 shows this version. It is possible to form the stiffening by simply patterning the grid structure at the tip areas during photolithography. The stiff tip areas can then be formed simultaneously with the support structure.

The thickness of the support structure was initially set to 4 μm. The spring stiff-

[4]Chapter 4 will show that Q for the current system in air is about 17.
[5]Chapter 4 will show that the low-frequency noise level is indeed about 1 nm.

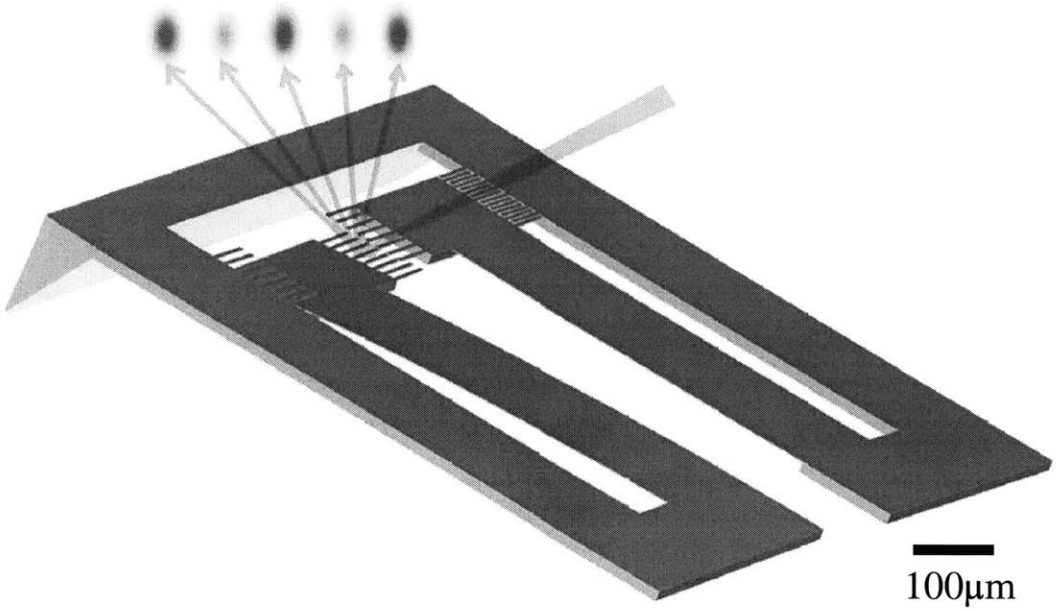

Figure 2-11: Concept of differential micromechanical sensor with stiffened tip areas.

ness of the support structure was estimated using finite element analysis[6] whereby a cantilever with the same length, width and material properties as the flexible sensor cantilever but a cross-section that is identical to that of the support structure was excited by a point-load of 0.1 μN applied at its tip. The resulting spring stiffness (applied force/observed tip deflection) was 1.66 N/m which is larger than the estimated spring stiffness of the sensor cantilever (0.036 N/m) by a factor of 46. Furthermore, to have an approximation for the comparative sensitivity of both structures to surface stress, the ratio of the spring stiffnesses can be scaled down by the ratio of the nominal thickness of the support structure (trench depth) to the sensor cantilever's thickness. This is because sensitivity of a cantilever-based structure to a point-load is scaled by $1/t^3$ whereas sensitivity to surface stress is scaled by $1/t^2$. Hence, the surface-stress-sensitivity of the support structure with a nominal thickness of 4 μm is approximately 12 times less than that of the sensor cantilever. To further decrease the surface-stress-sensitivity of the support structure, the second version of the de-

[6]Ansys was used due to problems encountered with ProEngineer while meshing/simulating the support structure.

vice was fabricated with 10 μm of nominal thickness which is expected to result in a surface-stress-sensitivity that is approximately 44 times less than that of the flexible sensor cantilever. The spring stiffness of the support structure with 10 μm nominal thickness was estimated to be 15.9 N/m by finite element analysis.

The next chapter describes the fabrication process of the designed device.

Chapter 3

Device Fabrication

This chapter describes the microfabrication of the device. In the last chapter, a few important issues about the fabrication of the device were mentioned. In this chapter, the details of the fabrication process flow is presented. The difficulties experienced and their remedies are discussed. The results of the fabrication are illustrated with scanning electron micrographs and optical images. The fabrication was performed in the cleanroom facilities, namely the Technology Research Laboratory (TRL) and the Integrated Circuits Laboratory (ICL) of the MIT Microsystems Technology Laboratories.

3.1 Fabrication process flow

Fig. 3-1 shows the main steps of the fabrication process. The fabrication comprised patterning of low stress silicon nitride with 3 photolithography steps. Hence 3 different masks were used[1]. Standard 4-inch, 520 μm-thick, double-side polished, silicon $\langle 100 \rangle$ wafers were used. Each photolithography step comprised 1-μm-thick resist spinning, pre-baking at 90°C for 30 minutes, UV light exposure[2] for 1.5 seconds, wet resist development, and post-baking at 120°C for 30 minutes.

As the first step of fabrication, the wafers were cleaned using a standard RCA

[1]Masks were prepared by Compugraphics on standard chrome plates using 0.25 μm beam diameter.

[2]TRL machine EV1 was used for alignment and exposure.

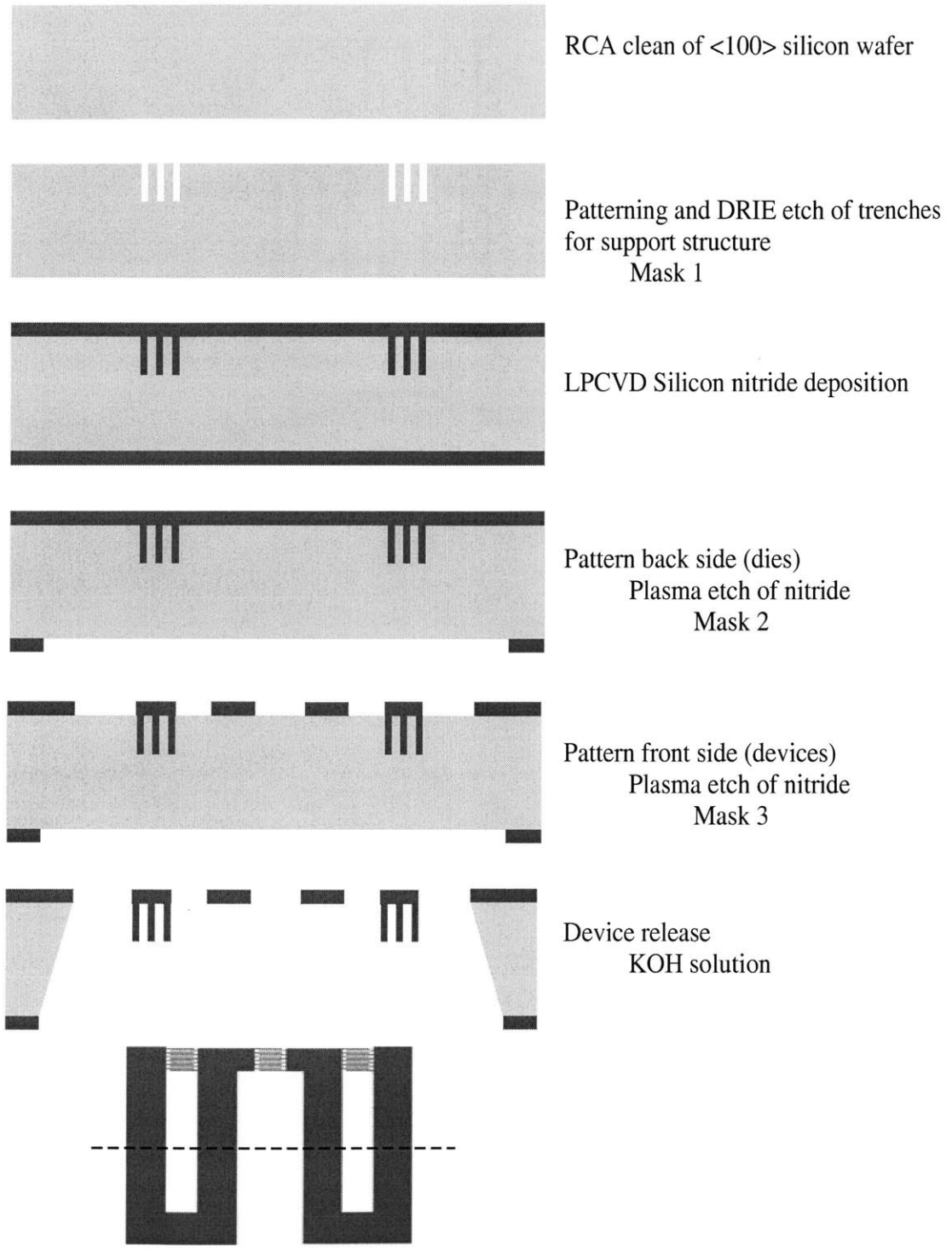

Figure 3-1: Fabrication process flow. Major steps of fabrication are shown.

process. The 2 μm-wide grid pattern of the support structure was defined by the first photolithography step. Then, 4 μm-deep trenches were formed by deep reactive ion etching (DRIE) of the silicon wafer in a time multiplexed SF_6/C_4F_8 plasma for 4 minutes. The photoresist was used as the etch mask. In a later version of the device, the trench depth was increased to 10 μm to further stiffen the supports. The DRIE etch was performed in the TRL machine STS using the *20-μm shallow etch recipe.* The photoresist was removed using a piranha clean (1:3 H_2O_2-H_2SO_4).

The next step was the low-pressure chemical vapor deposition (LPCVD) of low-stress silicon nitride. However, in the cleanroom facilities of MIT, a wafer that has gone through a DRIE process is not allowed in the VTR (the ICL machine used to deposit low-stress silicon nitride). This is because the DRIE utilizes C_4F_8 for side-wall passivation to enable high-aspect-ratio etches, and this residue contaminates the VTR. Hence, C_4F_8 must be removed before introducing the wafer into VTR. Unfortunately piranha clean does not remove this residue. To ensure complete removal, a thin layer of oxide was grown at 1100°C for 30 minutes (to burn the residue), and then stripped using a buffered oxide etch (BOE). An RCA clean was performed both before the oxidation and after the BOE etch.

Next, the wafer was coated conformally with 1 μm low stress silicon-rich (10:1 DCS:NH_3) silicon nitride to form the support structures and the 1-μm-thick cantilevers simultaneously. Individual dies were defined by a backside photolithography, followed by a plasma etch of the nitride in CF_4 for 360 seconds in the ICL machine AME. Again, the photoresist was removed using a piranha clean. During the plasma etch of the nitride, it was realized that CF_4 etches the photoresist. Over 360 seconds, 1-μm-thick photoresist was almost completely etched and the nitride underneath was attacked. This however is of minimal concern for the backside, since the backside nitride is used only as an etch mask for KOH and its exact thickness is not critical. However, on the front side, it is important to protect the nitride underneath the photoresist. Front-side nitride forms the devices, and hence its thickness must be controlled. Therefore, the thickness of the resist to be deposited on the front side was increased to 4.5 μm to ensure full protection of the nitride.

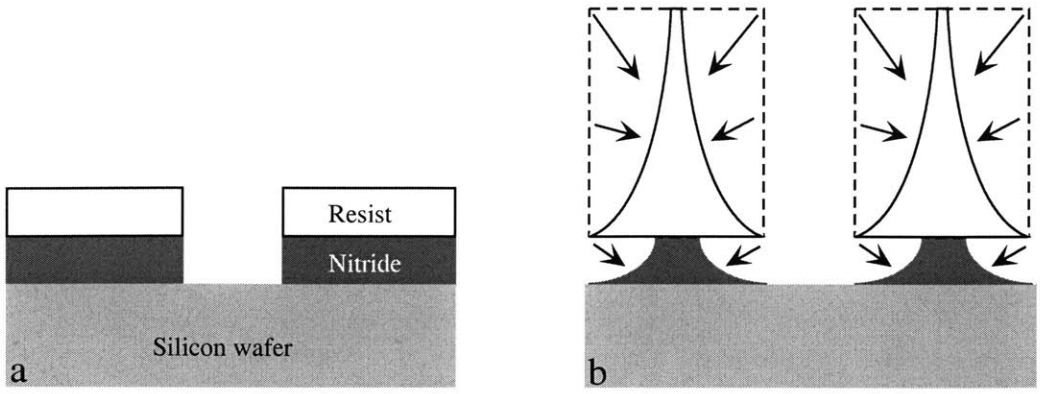

Figure 3-2: Deformation of ID finger cross-section due to thick resist. a) Ideal cross-section b) Deformed resist profile, and resulting finger cross-section.

The last photolithography step was performed to pattern the front side of the wafer to define the devices. This step was followed by the plasma etch of the nitride in CF_4. Thick resist prevented CF_4 from attacking the nitride, but resulted in an additional problem that is shown in Fig. 3-2. The ID fingers are 4 μm wide, and there is a 2-μm gap between them. Ideally, their cross-section must be perfectly rectangular. To enable this, the photoresist pattern after development must also be perfectly rectangular. As the resist thickness increases, it becomes more difficult to retain the resist cross-section. As shown in Fig. 3-2, the walls of the resist develop laterally and result in a non-ideal resist profile. This profile is disadvantageous because the edges of the resist become extremely thin and fail to protect the nitride underneath them during the plasma etch. As a result, the nitride cross-section imitates the profile of the resist that is resting above it. This is not desirable because the ID fingers must have flat surfaces to reflect a laser beam. The ID fingers that have nonuniform cross-sections can result in complicated interference patterns (if the laser beam interacts with the top sides of the fingers). This problem was alleviated by directing the laser beam to the back sides of the ID fingers (hence the device was flipped over to its back side for earlier experiments). Later on, the etch gas was changed from CF_4 to SF_6. It was realized that SF_6 has a much better selectivity for silicon nitride and does not attack the photoresist. Hence, the resist thickness was reduced back to 1 μm, and as

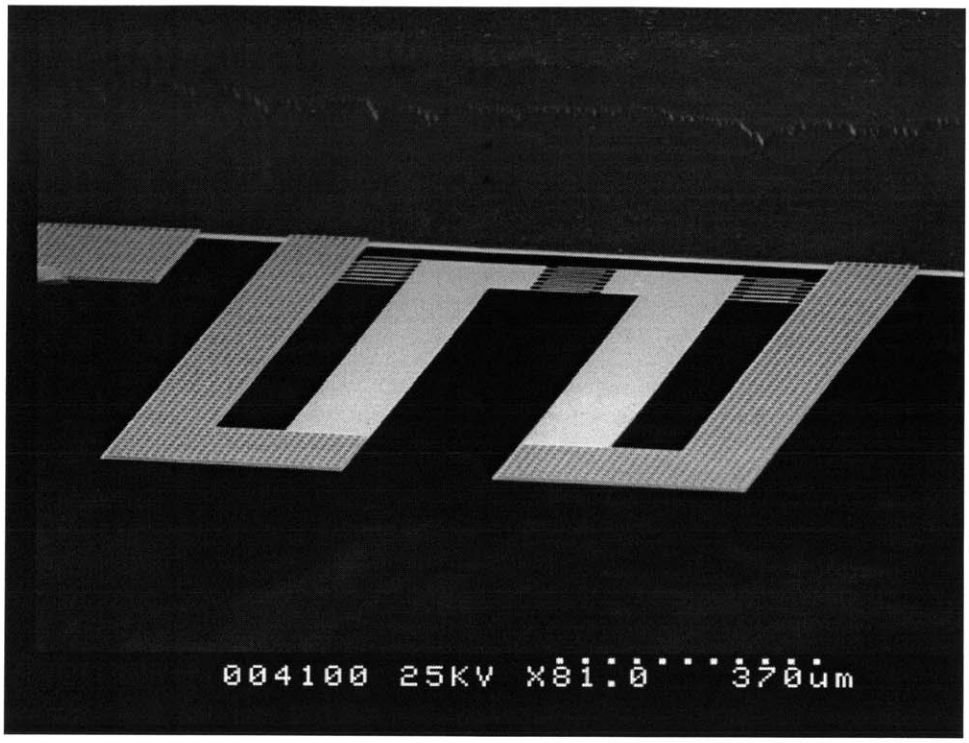

Figure 3-3: Scanning electron micrograph of the differential micromechanical biosensor.

a result the ID fingers with nearly perfect cross-sections were produced.

Finally, the devices were released with a wet etch of the bulk silicon. This is the last step of the fabrication process, and does not require a cleanroom environment. Hence, the wafers were taken out of the MTL clean room facilities and brought to the Media Laboratory to carry out the etch. The etch was carried out in a KOH solution (25% by volume) at 65°C over a period of 17 hours. The KOH solution was prepared in a glass beaker that was big enough to accommodate a 4-inch wafer. The beaker was placed in an acrylic water bath whose temperature was controlled using a Haake DC 10 unit. The solution was continuously stirred with a magnetic stirrer.

3.2 Fabrication results

Fig. 3-3 shows an SEM image of a completed device. Fig. 3-4 shows an SEM of the support-cantilever intersection and illustrates the step-change in thickness that

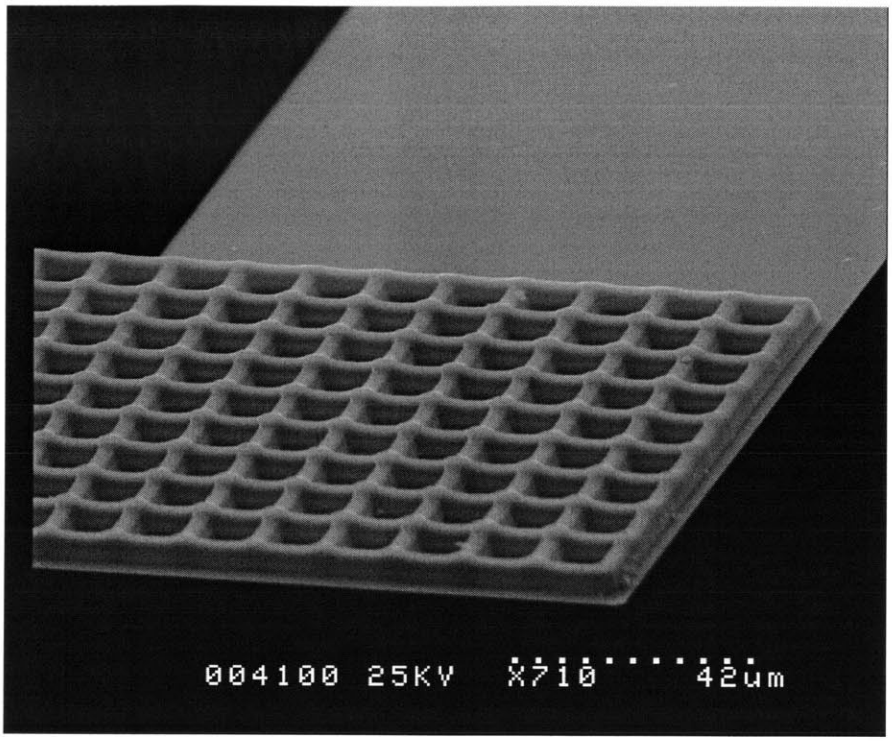

Figure 3-4: Scanning electron micrograph of the support-cantilever intersection.

occurs at the intersection[3]. The main reason for the particular *U-shaped* geometry of the device is ease of chemical functionalization. This particular design allows separate insertion of each cantilever into a pipette for fluidic delivery. Fig. 3-5 shows an optical image of the device before and after the insertion of one cantilever into a commercially available glass pipette.

[3]The SEMs in figures 3-3 and 3-4 were generated at the MIT ICL.

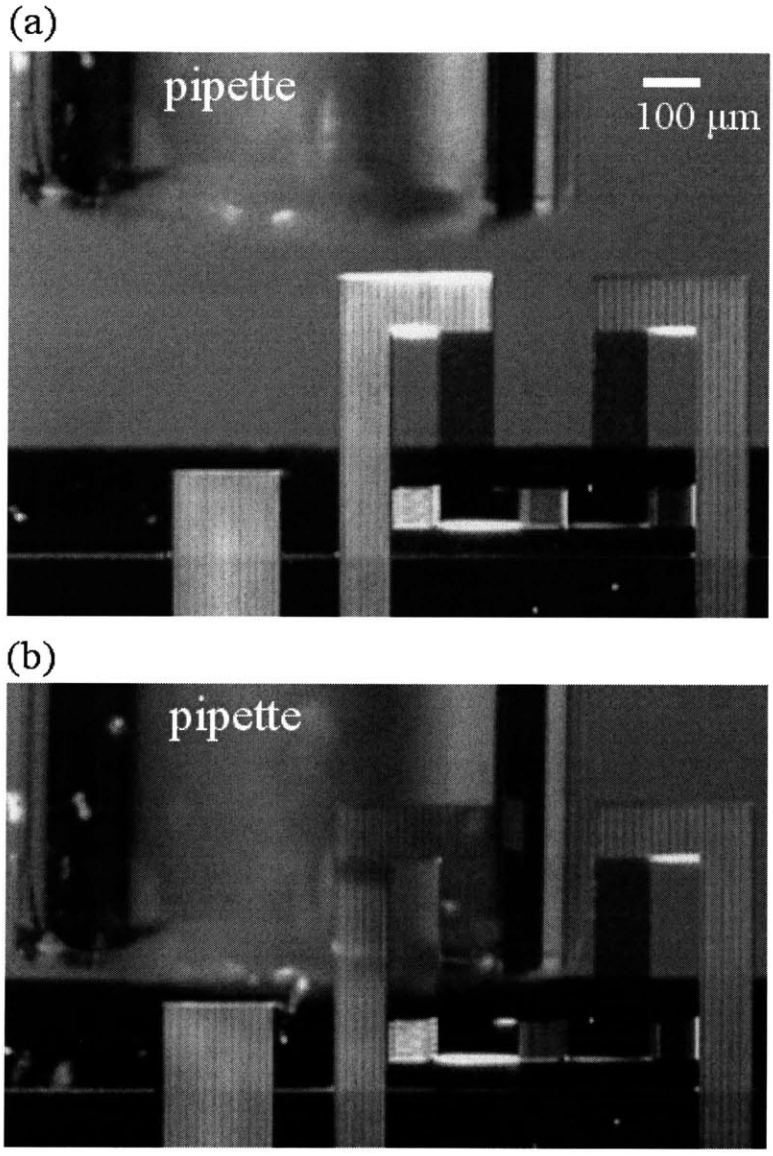

Figure 3-5: Insertion of a cantilever into a commercially available glass pipette a) before insertion b) after insertion.

Chapter 4

Device Characterization

This chapter describes the characterization of the differential micromechanical biosensor. The experimental setup comprising optical, fluidic and micromachined subsystems is presented. The calibration of the measured optical signal for deflection is described. The dependence of sensor response to geometrical parameters is investigated by using three cantilevers with different lengths and thicknesses. This also serves to verify the validity of Stoney's equation for the current sensor. The effectiveness of the differential sensor is analyzed in terms of similarity of the two adjacent cantilevers. The differential sensor's ability to suppress chemical and thermal background disturbances, i.e., its common-mode rejection is analyzed by changing the pH and the temperature in the detection environment. The sensor noise is analyzed, both at high and low frequencies. The chapter is concluded by presenting the application of the sensor to a model protein-ligand binding interaction, and verifying the results with a conventional biosensing technique.

4.1 Experimental Setup

The experimental setup comprises the fluidic chamber, optical components, and the data acquisition interface. Fig. 4-1 shows a schematic of the setup. The micromechanical sensor is placed in the fluidic chamber into which chemical solutions can be injected. A helium-neon laser (1126P, JDS Uniphase) is used to illuminate the ID

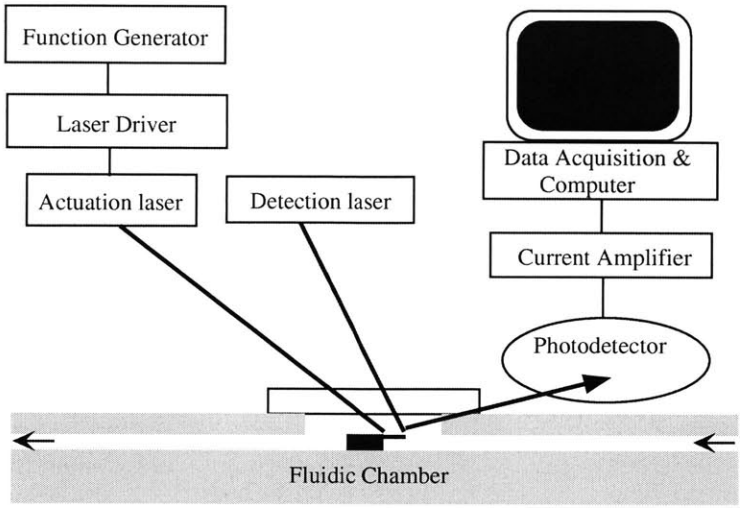

Figure 4-1: Experimental setup.

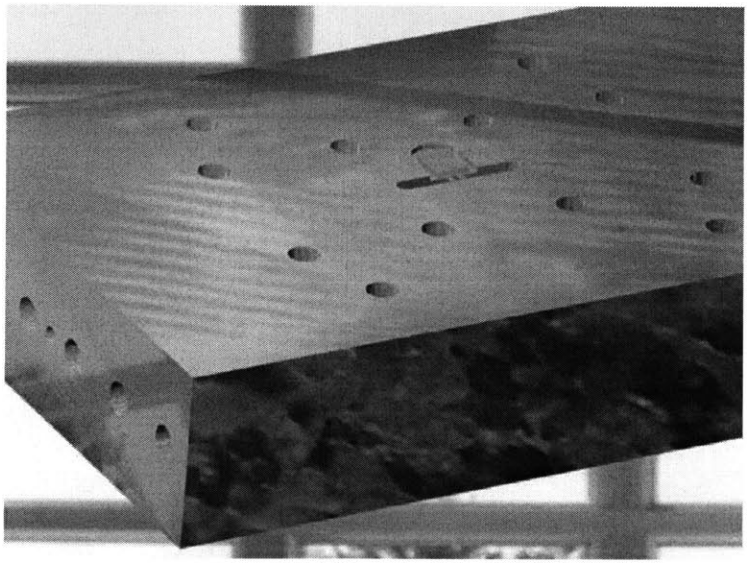

Figure 4-2: Stainless-steel fluidic chamber.

fingers of the sensor, and a silicon photodetector is used to measure the intensity of a particular diffraction mode. The photodetector output is converted from current to voltage using a Keithley 428 current amplifier. The resulting signal is acquired by a National Instruments BNC-2090 data acquisition interface and transfered to a computer which uses a Labview VI to collect and store data. A second laser source (Hitachi HL6501MG) was used to heat the base of one cantilever (the reference cantilever) and bias it to the most sensitive point of the interferometer for sensitive measurements.

The helium-neon laser, i.e., the detection laser has a wavelength of 632.8 nm and, a maximum power of 10 mW. The helium-neon laser was preferred due to its superiority over laser diodes in wavelength accuracy and stability (better than 1 Å). The second laser source, i.e., the actuation laser has a wavelength of 670 nm and a maximum power output of 30 mW. The power input to this laser diode was controlled with a ILX Lightwave LDX-3620 ultra low noise current source.

The photodetector is a silicon split-photodiode which enables detecting the intensities of two adjacent modes individually. During the optical alignment, the intensities of two adjacent modes were measured simultaneously as the reference cantilever was actuated by the secondary laser source. This was performed to verify that the two intensities change in opposite directions, and hence to confirm that the interferometer operates as expected. However, during the actual experiments only one mode was used.

The fluidic chamber (Fig. 4-2) consists of a channel (1 mm wide and 1 cm long) and a housing that accommodates the micromachined sensor die. A glass piece is screwed onto the chamber to hold the die in place, and also to allow the laser beams into the chamber. The chamber is machined out of stainless-steel to minimize spatial temperature gradients, and to prevent rusting. There are other channels in addition to the one that is used to deliver chemical solutions. These channels enable to run water through the chamber and circulate it through a temperature control unit. This feature can be used for future biological experiments that require a specific temperature. Within the context of this thesis, it was only used to test the sensor's ability to

suppress thermal disturbances. The author would like to re-acknowledge Thomas Burg for his indispensable effort in fluidic chamber's fabrication and in the general improvement of the experimental setup.

4.2 Calibration

The optical signal that represents the absolute or differential cantilever deflection is in the units of volts as acquired by the computer (Eq. 4.1)

$$I = Asin^2\Big(\frac{2\pi}{\lambda}\xi\Big). \tag{4.1}$$

Here, I is the modal intensity in volts (after having been coverted by the Keithley current amplifier), A is amplitude in volts, ξ is deflection in nanometers, and λ is illumination wavelength in solution, i.e., 480 nm (due to water's refractive index of 1.33). The signal was calibrated for deflection (in nanometers) by solving Eq. 4.1 for ξ:

$$\xi = \frac{\lambda}{2\pi}sin^{-1}\Big(\sqrt{\frac{I}{A}}\Big). \tag{4.2}$$

In the beginning of each experiment, the reference cantilever was bent gradually using the actuation laser to confirm the behavior described by Eq. 4.1, and to determine the amplitude A. This was accomplished by modulating the power of the actuation laser with a triangle wave. The power of the laser was measured to vary between 0-15 mW (power-equivalent minimum-maximum of the triangle wave) [1]. Fig. 4-3 shows the intensity change of a mode (generated by the differential ID fingers) as the reference cantilever was heated by the actuation laser. The resulting sin^2 behavior indicates that the bending i.e., the variation in ξ is linear with actuation laser power [41].

Here, in accordance with Eq. 4.1, the distance between the trough and the crest of the of the sin^2 curve corresponds to a quarter of the illumination wavelength in

[1]Measurement was done with a Coherent Labmaster laser detector.

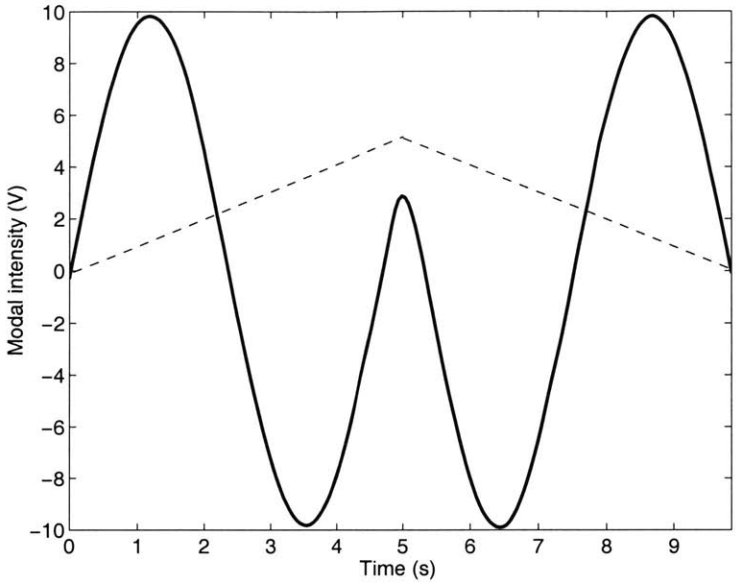

Figure 4-3: Differential cantilever bending in solution as the actuation laser gradually heats the reference cantilever. Actuation laser is modulated with a triangle wave indicated with the dashed curve.

solution i.e. ~120 nm. The deflections that result from biomolecular interactions are much smaller (on the order of 10 nm). Due to the nonlinear nature of the optical response (the sin^2 behavior), a 10 nm deflection can yield different optical responses depending on the operation point on the curve, i.e., the initial distance between the two cantilevers. Hence, for accurate calibration, it is essential to know the operation point during the experiment. In addition, the trough and the crest of the curve are the most insensitive points. Hence, it is safe to expect a small deflection and set the operation point to the most sensitive point of the curve, i.e., half-way between the trough and the crest, and, avoid the crest and the trough region as much as possible. Accordingly, before each experiment, the operation point was set at the most sensitive point of the sin^2 curve (odd multiple of $\lambda/8$) by manually adjusting the power input to the actuation laser.

It is important to note that the exact distance between the two ID finger sets is not known since the initial distance between them (without any actuation) is not known and may not necessarily be zero. After the biasing, it is only known that the distance is

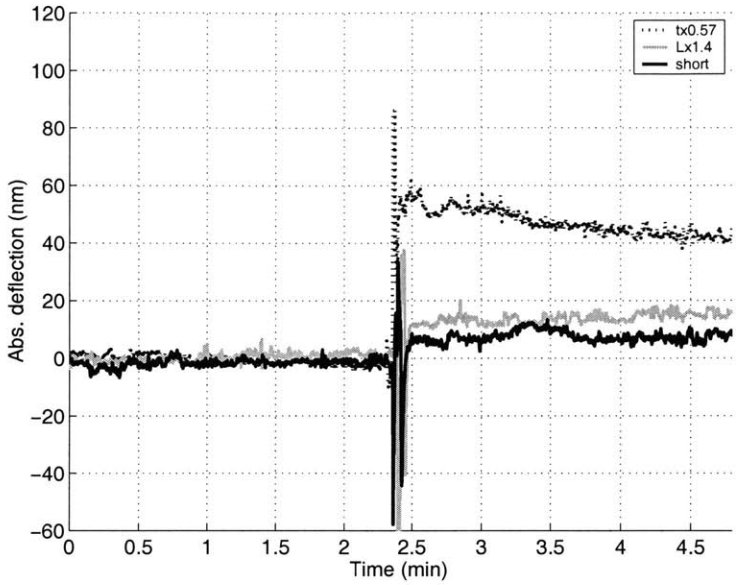

Figure 4-4: Absolute deflection of 3 different cantilevers upon a pH change from 6 to 7.

an odd multiple of $\lambda/8$. This is sufficient since during the experiment, the investigated quantity is the *deflection* of one ID set (one cantilever) with respect to the other, not the exact distance between the two. Hence, in all figures showing experimental bending results, the initial deflection value was arbitrarily and intentionally set to zero.

4.3 Verification of the surface-stress model

In order to investigate the validity of the surface stress model described in Chapter 2, the geometrical properties of the sensor, namely its length and thickness were varied. The material properties shown in the Stoney's equation are not expected to change across a wafer. Three different devices were fabricated and tested: 1) short & thick, 2) long & thick, 3) short & thin. Here, short and long represent length values of 374 μm and 524 μm respectively. Thin and thick represent thickness values of 0.57 μm and 1 μm respectively.

It is known that a silicon nitride surface reacts chemically to pH changes in the

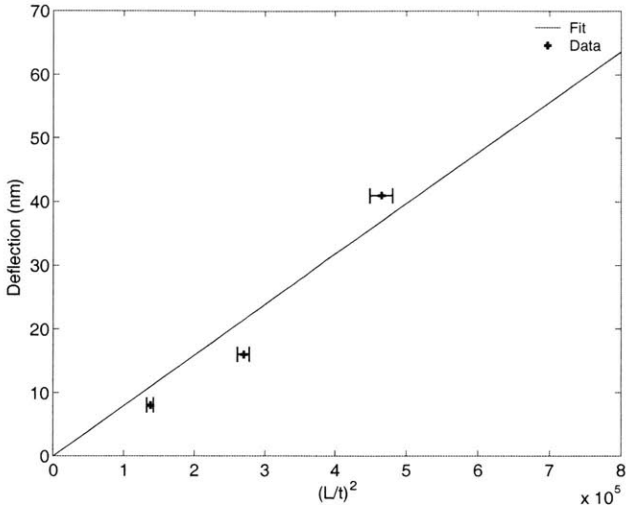

Figure 4-5: Geometrical dependence of absolute cantilever deflections shown in Fig. 4-4.

solution that surrounds it[2] [45]. It has also been shown that this reaction generates a surface stress that can bend a micromachined cantilever with different top (gold) and bottom (silicon nitride) surfaces [21]. Devices were coated with 20 nm of gold (with 1 nm of titanium as adhesion layer) using e-beam evaporation, and the absolute response of each sensor to pH was tested. A device was placed in the fluidic chamber and two different phosphate buffer solutions (with pH values of 6 and 7) were sequentially injected into the chamber. Fig. 4-4 shows the response of each device to the same pH variation.

Fig. 4-5 shows the steady-state deflection values plotted against the lumped geometrical parameter of the Stoney's equation, i.e., $(L/t)^2$. The horizontal error-bars represent the uncertainty in the geometrical parameters. These are ± 1 μm error in length (possible error during photolithography), and ± 10 nm error in thickness (thickness deviation across wafer as measured in MIT ICL (Integrated Circuit Laboratory)). Also displayed is a linear fit to these three points and the origin. For Stoney's equation to perfectly apply, all three points must be on the line, which is clearly not the case (even with the horizontal error bars in consideration). This is be-

[2]It will be seen later that this reaction also has reversible characteristics.

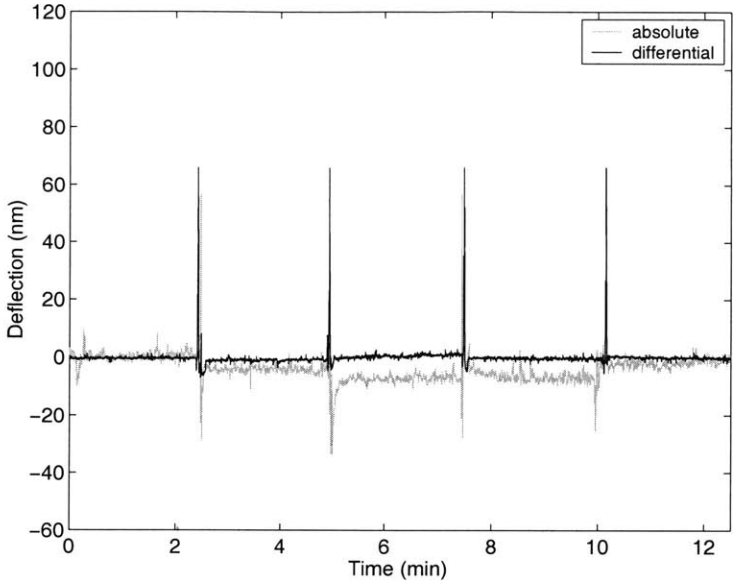

Figure 4-6: Chemical disturbance rejection. Spikes indicate sequential injection of phosphate buffer solutions with pH values of 7, 6, 7 and 8.

cause the surfaces of the three cantilevers may not be absolutely identical, and hence, the effect of the pH change on each surface may not be exactly the same. However, the points are close enough to the line to suggest that the Stoney trend is roughly correct, i.e., the sensor is detecting a chemical event that is almost independent of the cantilever geometry. Consequently, using Stoney's equation to determine an effective surface-stress that represents a specific chemical reaction on a surface is a convenient approximation.

4.4 Common-mode rejection

The main advantage of the dual-cantilever device is the inherent common-mode rejection. Due to its differential nature, the sensor is able to suppress disturbances that equally influence the two adjacent cantilevers. Two main disturbances to the sensor are chemical changes in the environment and the bi-material effect of temperature changes, both of which can cause effective surface stresses that can bend the cantilevers.

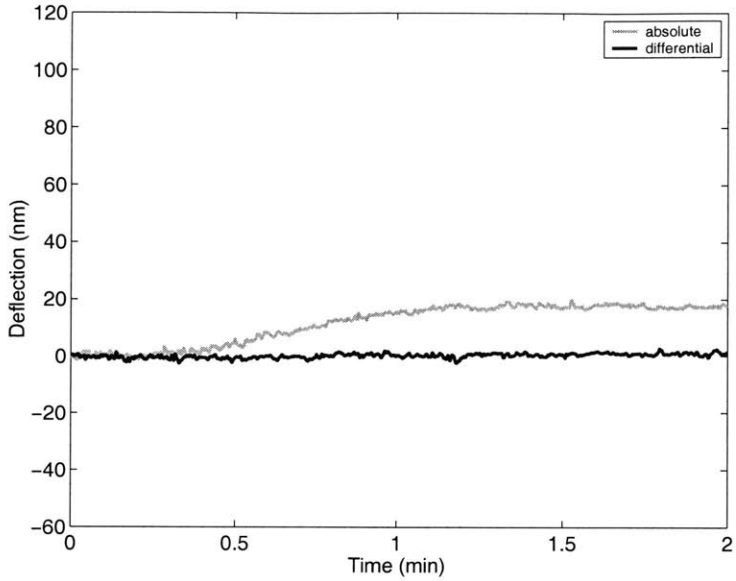

Figure 4-7: Thermal disturbance rejection. Absolute and differential bending responses to a change in the temperature of the solution.

The sensor's ability to suppress nonspecific chemical disturbances was tested by observing its response to pH variations (Fig. 4-6). A device was placed in the fluidic cell and equilibrated in a 100 mM phosphate buffer solution with pH 8. The period up to time=2.5 min. represents response to pH 8. From that point on, each spike represents sequential injection of solutions with pH values 7, 6, 7 and 8. Fig. 4-6 shows that the differential detection significantly reduces the effect of pH changes, and results in a more stable response. Fig 4-6 also shows that differential detection can suppress the transients following injections.

It was discussed in Chapter 2 that temperature changes in solution can induce significant cantilever bending due to the bi-material effect at the silicon nitride-gold interface. It was shown analytically that for gold thicknesses (~20nm) that are much smaller that the cantilever thickness (~ 1 μm), the bi-material effect can be represented by an effective surface stress. Accordingly, bending caused by a temperature change cannot be differentiated from that caused by a chemical/biological interaction. Hence, for reliable biomolecular detection, it is essential to suppress the effect of temperature changes. In experiments involving single cantilevers, temperature of the solution must

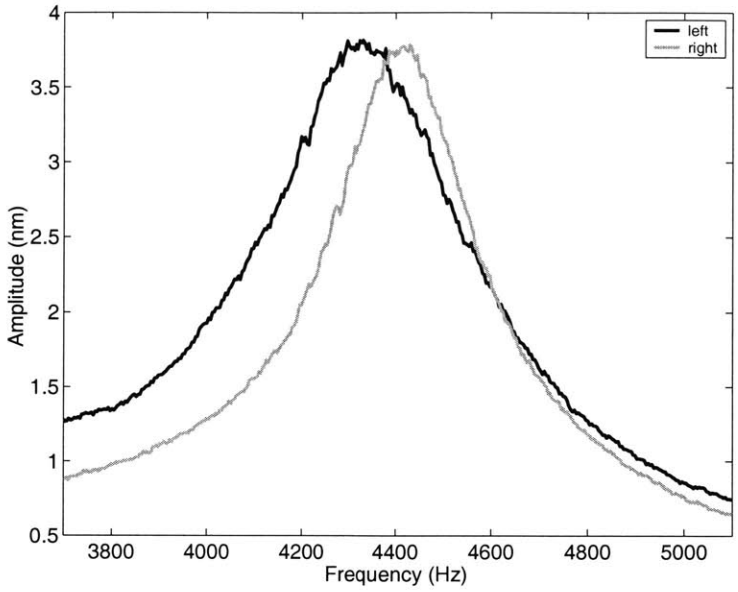

Figure 4-8: RMS vibration amplitude of each cantilever in air versus the drive frequency of the actuation laser.

be precisely controlled [27]. Fig 4-7 shows that differential detection suppresses the effect of a temperature change that absolute detection exhibits. To perform this experiment, a device was placed in the fluidic chamber, the chamber was connected to a temperature controlling unit, and the unit was commended to perform a step-change of 0.3 °C.

The differential effectiveness depends on the similarity of the two adjacent cantilevers. For an ideal differential sensor, the two adjacent cantilevers must be identical. However, errors during fabrication and variations in the two surfaces can cause differences between the two cantilevers. The similarity of the two cantilevers was investigated by comparing their natural frequencies. The natural frequencies were measured by modulating the actuation laser with a sine wave and gradually increasing its frequency. The measurements were performed in air to achieve large deflections at resonance. Fig. 4-8 shows that the two natural frequencies differ by 85 Hz, which corresponds to a variation of about 2%. The natural frequency depends both on mass and stiffness. However, the response to surface stress depends only on stiffness. Thus, for a worst-case analysis of the effect of natural frequency difference, all of the

observed variation is assumed to arise from stiffness variation.

From the Stoney's equation, one can define an effective *Stoney stiffness*:

$$k = \frac{\sigma}{\delta} = \frac{E}{3(1-\nu)}\left(\frac{t}{L}\right)^2. \tag{4.3}$$

The stiffness ratio of the two adjacent cantilevers is then

$$\frac{k_1}{k_2} = \frac{\dfrac{E_1}{3(1-\nu_1)}\left(\dfrac{t_1}{L_1}\right)^2}{\dfrac{E_2}{3(1-\nu_2)}\left(\dfrac{t_2}{L_2}\right)^2}. \tag{4.4}$$

The natural frequency ratio of the two cantilevers is

$$\frac{\omega_1}{\omega_2} = \frac{\sqrt{\dfrac{E_1}{\rho_1}}\dfrac{t_1}{L_1^2}}{\sqrt{\dfrac{E_2}{\rho_2}}\dfrac{t_2}{L_2^2}}. \tag{4.5}$$

Substituting 4.5 into 4.4 yields

$$\frac{k_1}{k_2} = \frac{t_1}{t_2}\frac{1-\nu_2}{1-\nu_1}\sqrt{\frac{E_1\rho_1}{E_2\rho_2}}\frac{\omega_1}{\omega_2}. \tag{4.6}$$

Note that Eq. 4.6 relates the natural frequencies to *Stoney stiffnesses*, not to the *spring stiffnesses* since the primary reason for cantilever bending is surface stress, not a point load applied at the tip.

There is no evidence to suggest that material properties of a thin film can change across a wafer, especially over a distance of 100 μm (the distance between the two cantilevers). However, the thickness of the film can change across the wafer. The thickness of the deposited silicon nitride film was measured at various points on a wafer. The maximum thickness variation from one end of the wafer to another was measured to be 15 nm (for 1 μm nominal film thickness). Assuming a linear variation in thickness from one end of the wafer to the other yields an expected maximum thickness variation of 0.15 Å over 100 μm. Thickness measurements performed on

two adjacent cantilevers yielded differences that are less than 0.1 Å or 0.001 %. Accordingly, the thickness variation from one cantilever to another can be safely considered negligible. Consequently, Eq. 4.6 suggests that the Stoney stiffnesses of the two cantilevers should not differ by more than 2 %. Again, this is based on the conservative assumption that the difference in natural frequencies only results from that in the stiffnesses.

It is important to remember that the differential effectiveness analysis is only based on the differences in the mechanical properties (material and geometrical) of the two cantilevers. It does not consider any surface effects; the surfaces of the two cantilevers may not be exactly the same. During a chemical/biological reaction, how the two surfaces might differ in the way they react chemically to the presence of a surrounding solution is not known. However, since the two cantilevers are not only from the same wafer, but also only 100 μm apart from each other, it is expected that the differences in their surfaces are minimal. As will be demonstrated later, differential effectiveness was also investigated during biological experiments, by functionalizing both cantilevers with control molecules, and observing that the differential deflection is insignificant.

4.5 Noise Analysis

The differential micromechanical sensor was built to detect motions that are on the order of a nanometer. Hence, the effectiveness of the sensor is evaluated by its ability to detect motions that are as small as possible. A noise analysis was performed to investigate the limitations of detection and determine the minimum detectable deflection. The sensor's response to background noise was measured in the absence of any actuation. This was achieved by recording the response over a period of 10 seconds with a sampling frequency of 100,000 Hz. After calibrating the response for deflection, its power spectral density was determined using the MATLAB command *spectrum*[3].

[3]with nfft parameter being 2^{18}.

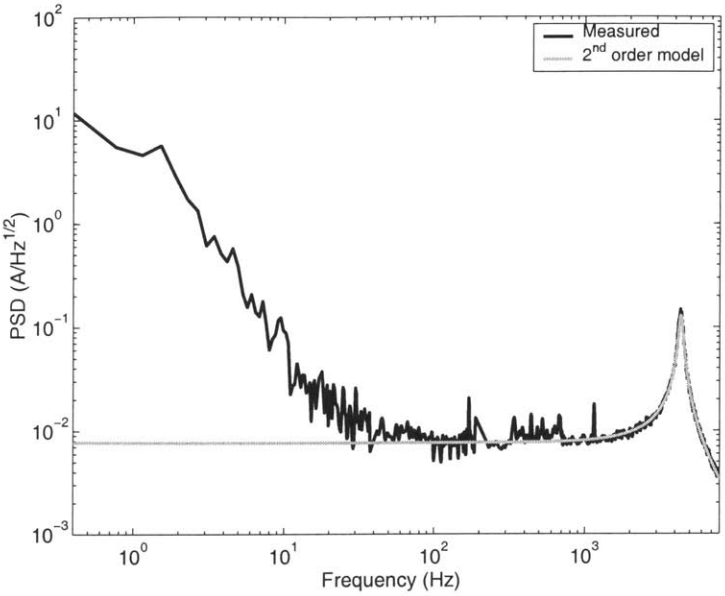

Figure 4-9: Power spectral density of the differential cantilever deflection in air (Measured). 2^{nd} order fit is an ideal harmonic oscillator driven by the thermomechanical noise of the sensor.

Fig. 4-9 shows an overlay of the measured response's spectrum in air and the magnitude of the frequency response of an ideal second-order harmonic oscillator driven by the cantilever's K_bT-level thermal energy [41]:

$$X(\omega) = \sqrt{\frac{\frac{4K_bT}{K\omega_n}}{Q\left(1-\frac{\omega^2}{\omega_n^2}\right)^2 + \frac{\omega^2}{Q\omega_n^2}}}. \tag{4.7}$$

Here, Q, K, and ω_n represent the quality factor, stiffness, and the fundamental natural frequency of the cantilever respectively. K_b, T, and ω stand for the Boltzmann constant, room temperature and excitation frequency, respectively.

Eq. 4.7 assumes that the low-frequency response of the cantilever is dictated only by its thermomechanical noise level predicted by Eq. 4.8:

$$\delta = \sqrt{\frac{4K_bT}{QK\omega_n}}. \tag{4.8}$$

The measured spectrum shown in Fig. 4-9 has flicker noise combined with second-order dynamics. Fitting the second-order dynamics of the measured spectrum to Eq. 4.7 for $\omega_n = 2\pi \cdot 4375$ rad/s reveals: $Q = 16.75$ and $K = 0.061$ N/m. From Chapter 2, the theoretical stiffness of the cantilever based on the dimensions and material properties is $K = 0.036$ N/m [42]. The difference between the two stiffness values may be a result of the deviation of the material properties from the tabulated ones. In literature, it is possible to find values for the Young's modulus of silicon-rich nitride that vary from 180 GPa [36] to 270 GPa [46].

The fit of Eq. 4.7 shows that the measured response is the thermomechanical noise level of the cantilever over the frequency range 40-1000 Hz. This value as calculated using Eq. 4.8 is ~ 0.01 ÅHz$^{1/2}$. For applications in this frequency range, only the thermomechanical noise of the cantilever limits the resolution, i.e., the sensor can detect motions with sub-angstrom precision. However, the primary intention for the use of this sensor is biosensing. Many biologically significant chemical reactions occur over minutes or tens of minutes. Unfortunately, at those time scales (at lower frequencies), thermomechanical noise is no longer the limit. As Fig. 4-9 shows, for frequencies lower than 40 Hz, the resolution is dictated by flicker or $1/f$-type noise. Integration of the low-frequency section of the spectrum reveals a noise level of approximately 1 nm, a value much larger than the thermomechanical noise level. Hence, the low-frequency noise of the sensor was investigated separately, and in greater depth [47].

To investigate the low-frequency noise, the behavior of the sensor was observed over a longer period of time. Since the sensor is intended for biological experiments, it is more realistic to measure the noise in an aqueous environment. A device was placed in the fluidic chamber and phosphate buffer was injected into the chamber. The behavior of the device was monitored (both with absolute and differential ID finger sets) over a period of 1 hour. A low-pass filter was used at the output of the photodetector to attenuate noise components above 1 Hz, since responses faster than 1 second are not common in biological reactions. Fig. 4-10 shows the absolute and the differential cantilever response over time. The absolute response has significant drift,

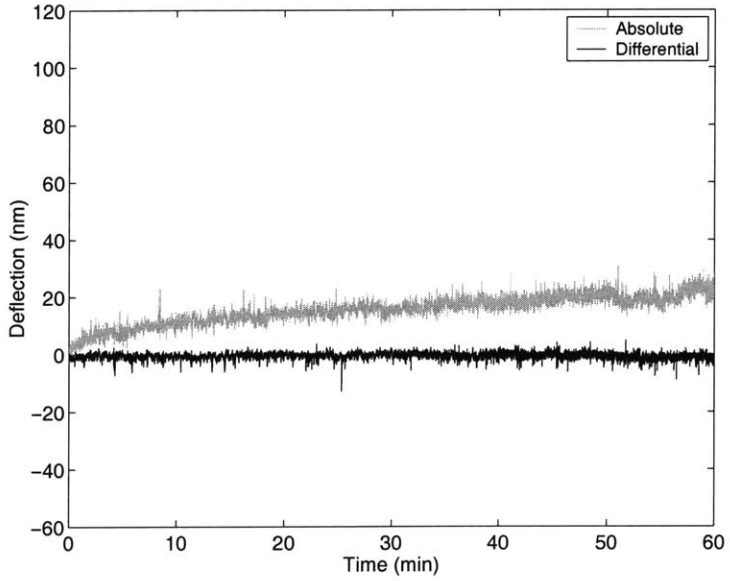

Figure 4-10: Absolute and differential cantilever response in phosphate buffer over 1 hr.

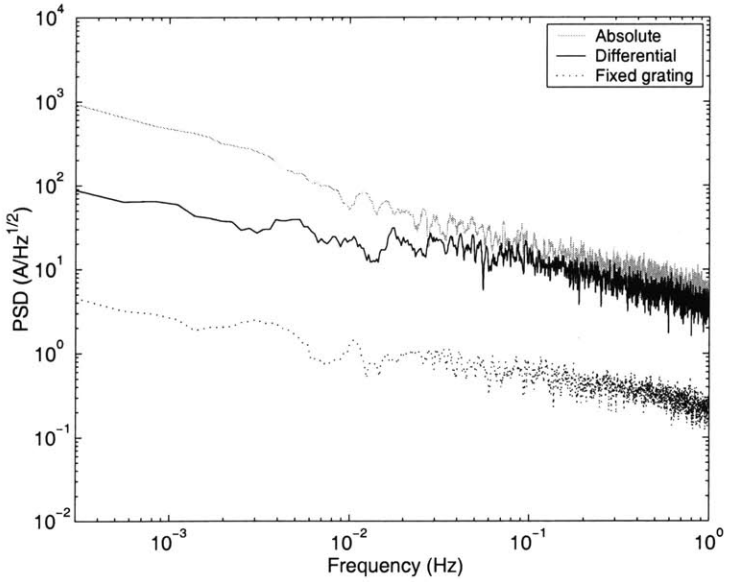

Figure 4-11: Power spectral density of absolute and differential cantilever bending in comparison with the deflection-equivalent PSD of a fixed diffraction grating response.

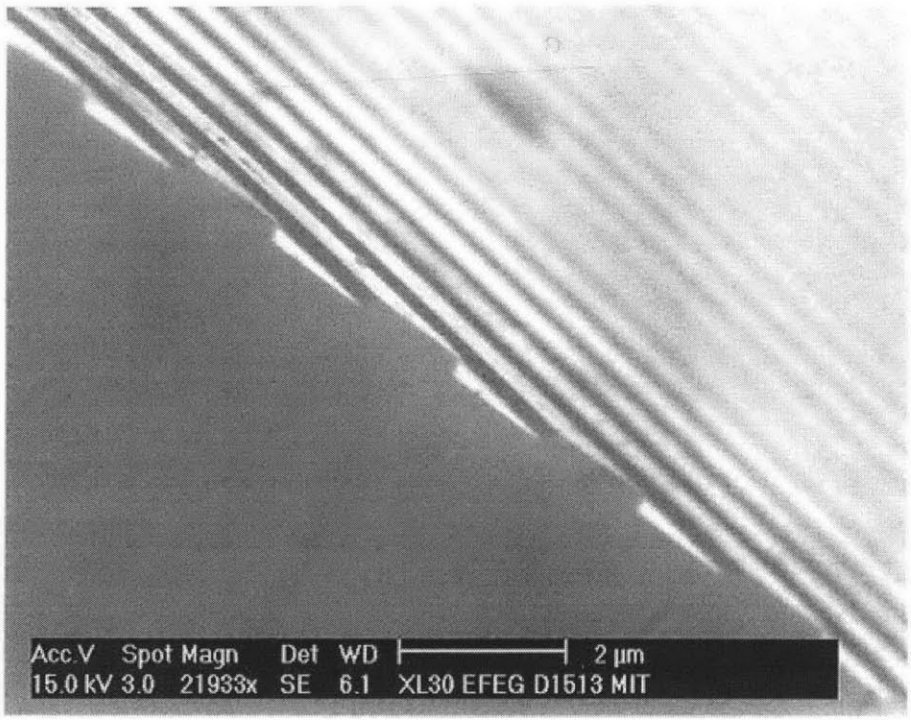

Figure 4-12: Scanning electron micrograph of the diffraction grating with fixed depth.

and some unsteadiness (e.g. time=52 min). As expected, the differential response has no drift. To assess the frequency dependence of the two responses, the power spectral densities (PSD) of both signals were calculated. Fig. 4-11 shows that the differential response reduces the low-frequency noise by as much as an order of magnitude (at 0.0003 Hz), and that differential detection is advantageous for measurements that require long time. The integration of the PSDs reveal RMS deflection values of 49 Å for absolute response and 10 Å for differential response.

Despite the fact that the differential detection significantly lowers the low-frequency noise, it does not eliminate it. Hence, it is necessary to determine whether it is caused by the optical detection system or physical motion of the cantilevers. Fig. 4-11 also shows the low-frequency noise of a diffraction grating with fixed depth in phosphate buffer. The grating was fabricated by patterning 210 nm of thermally grown oxide on silicon. The pattern of the grating is the same as that of the ID fingers of the sensor (Fig. 4-12). The grating was coated with a 20 nm gold layer (with 1 nm of titanium

as adhesion layer)[4] and placed in the fluidic cell. Since the grating has fixed depth, the measured response excludes deflection noise. Here, the possible components of the noise are fluctuations in the intensity and wavelength of the laser, those in the refractive index of the solution in the grating, and also the electronic noise of the devices used in the experimental setup. Hence, this measurement demonstrates the extent to which the optical and the electronic components of the detection system contributes to the overall noise. To enable comparison with the cantilever response, the response of the fixed grating was calibrated for an *effective deflection.* The calibration was performed by solving the argument of Eq. 4.1 for virtual variation in ξ that would cause an equal change in modal intensity to that caused by a small change in laser wavelength in the fluidic chamber:

$$\Delta\xi = \xi_0 \frac{\Delta\lambda}{\lambda_0}. \tag{4.9}$$

Here, ξ_0 is the fixed depth of the grating (210 nm), λ_0 is the detection laser wavelength in water (476 nm), and $\Delta\lambda$ is a perturbation in laser wavelength. The dependence of modal intensity on laser wavelength was determined by sequentially injecting fluids of known refractive indices (water and ethanol) [48] into the fluidic chamber and observing the photodiode output. Since the depth of the grating is known (verified with AFM), so is the corresponding biasing point of the interferometer. At 210 nm, the dependence of the modal intensity on refractive index changes is quite linear (even for a change from water to ethanol, which is far more severe than small variations that could occur over time in a buffer solution (PBS) that is mostly composed of water). The signal was then recorded over time, while the grating was immersed in phosphate buffer. The deflection-equivalent signal was calculated using Eq. 4.9 and by realizing that for a small perturbation Δn in the refractive index n_0:

$$\frac{\Delta\lambda}{\lambda_0} \cong \frac{\Delta n}{n_0}. \tag{4.10}$$

The PSD of the resulting signal was again calculated off-line. The comparison of the

[4]Deposition rates were 0.2 Å/s, and 0.1 Å/s for Au and Ti respectively.

PSD of the fixed grating with those of the differential and the absolute cantilever responses indicates that most of the low-frequency sensor noise is due to cantilever deflection. The comparison of the absolute and the differential PSDs was already suggesting this, it however was not sufficient to explain the source of the differential sensor noise. The fixed grating experiment shows that the deflection-equivalent RMS noise contributed by the detection system alone is only 0.5 Å over 0.0003-1 Hz.

The frequency content of the differential bending response is very similar to that of the fixed grating, i.e., the slopes of both responses are about $1/f$ (on $Å^2$/Hz scale). The fixed grating response contains the noise of electronic and optical components of the experimental setup. Hence, it is plausible for it to assume a trend that is close to $1/f$ noise. However, the exact reason for the differential bending noise to follow the same trend remains unclear. The origin of the surface stress that causes cantilever bending is not completely understood and hence, its is difficult to predict its frequency dependence.

4.6 Application to biomolecular detection

The next step is to test the sensor's ability to perform label-free and inherently differential detection of biomolecules, especially proteins. To demonstrate this, a model receptor-ligand binding experiment was performed. The experiment resembles directly the differential response between a surface that allows the binding, and a neighboring one that does not. The chosen model system was biotin-streptavidin binding. This is a very strong binding reaction very commonly used by biochemists to cross-link various molecules to surfaces [49].

The top side of the device was coated with 20 nm of e-beam deposited gold. The gold-coated sides of both the reference and the sensing cantilevers were passivated with thio-modified polyethylene glycol (PEG). PEG is a well-known molecule for repelling proteins and is commonly used to block protein adsorption onto surfaces. The passivation was performed immediately after gold deposition by inserting the device into a PEG solution (1 mg/ml in water). The silicon nitride surface of the sensing

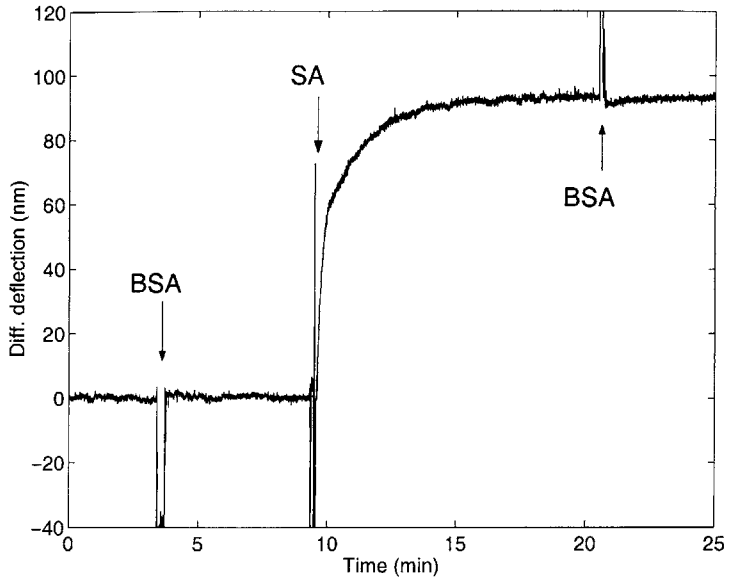

Figure 4-13: Differential micromechanical detection of biotin-streptavidin binding.

cantilever was functionalized with biotin-labeled bovine serum albumin (bBSA), by inserting the cantilever into a glass pipette containing the bBSA solution. Similarly, the nitride surface of the reference cantilever was blocked with bovine serum albumin (BSA). Since both the top and the bottom surfaces of the reference cantilever are blocked (with PEG and BSA), no specific binding to this cantilever is expected to occur. Both BSA and bBSA were dissolved in phosphate buffered saline (PBS) at a concentration of 5 mg/ml. The bond between BSA and the nitride surface is nonspecific, i.e., BSA is known to bind not only to silicon nitride but to a variety of surfaces (silicon, glass, quartz) and is frequently used by biologists to block empty spots on surfaces.

Following the functionalization, the device was placed in the fluidic chamber and allowed to equilibrate in a BSA solution (100 μg/ml in PBS). Several BSA injections were performed to form a baseline and to verify the stability of the sensor. A streptavidin (SA) solution (700 μg/ml) was injected to initiate biotin-streptavidin binding on the sensor cantilever. Fig. 4-13 shows the differential cantilever bending over the course of the experiment. Injecting a BSA solution at time=3.5 min caused negligible response (after the peak that represents the injection transient). SA injection

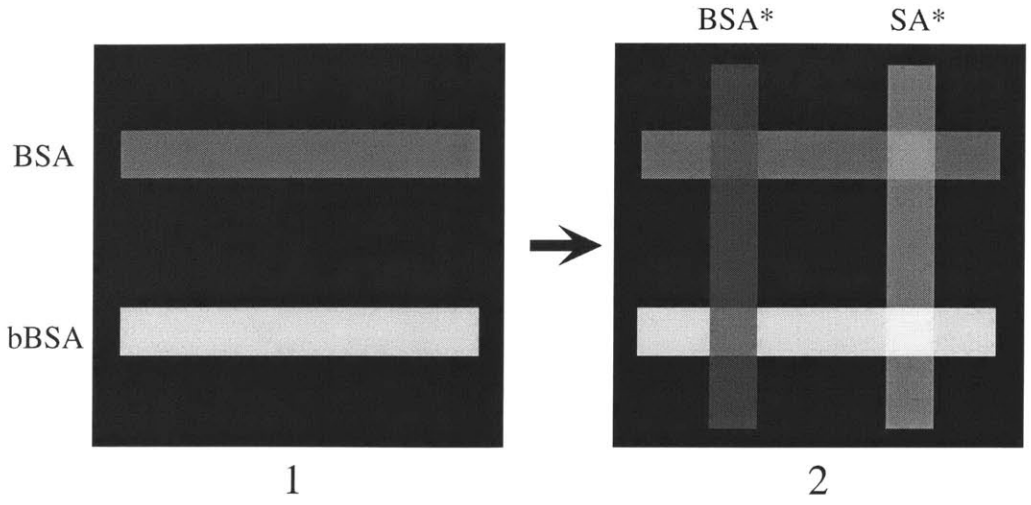

Figure 4-14: Detection of biotin-streptavidin binding using fluorescence microscopy. Stars represent fluorescent labels.

at time=9 min resulted in 92 nm of differential cantilever bending, or 0.04 N/m of differential surface stress according to Stoney's equation. The differential bending resulted from binding of SA to bBSA that was present only on one of the sensor cantilever's surfaces, and not on either surface of the reference cantilever.

The experiment was verified using fluorescence microscopy on an identical silicon nitride surface. This was done to confirm the binding of BSA and bBSA to silicon nitride. Also, it is desirable to verify that the biotin-streptavidin binding occurs on a silicon nitride surface. The experiment was performed on a quartz surface which had been coated with the same silicon nitride that was used to fabricate the cantilevers. Fig. 4-14 illustrates the experiment schematically.

First, the surface was functionalized with BSA and bBSA (both at 1 mg/ml) in the form of two parallel horizontal stripes. This was accomplished by a PDMS structure with parallel channels etched into it. The structure was brought to contact with the nitride-coated quartz surface and, BSA and bBSA solutions were flown across two separate channels. The PDMS structure was left on top of the quartz-nitride surface for 35 minutes with the channels filled. This is about the time that was used for all functionalization steps mentioned in this thesis. Then, the PDMS structure was separated from the surface, rotated 90°, and again brought to contact with

the surface. This time, its channels were filled with solutions of fluorescent-labeled streptavidin and BSA (0.5 mg/ml). FITC was the specific fluorescent die that was used to label both SA and BSA. Both SA and BSA are commercially available and can be purchased with or without FITC labels[5].

Fig. 4-15 shows that the greatest fluorescence signal comes from the lower right square (location 2,2) which is the surface that accommodates the bBSA-streptavidin interaction. This experiment shows that both BSA and bBSA stick to silicon-rich silicon nitride. It also confirms that streptavidin selectively binds to bBSA and that this binding occurs on the silicon nitride surface.

[5]All chemicals were purchased from Sigma, except for thiol-PEG which was purchased from Rapp Polymere GmbH, Germany.

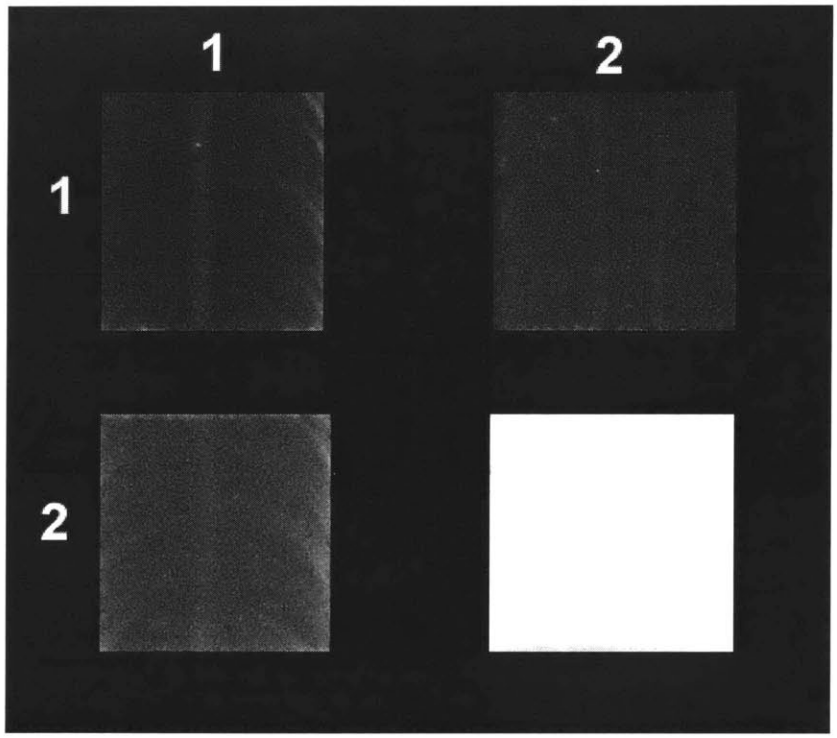

Figure 4-15: Fluorescence microscopy readout of biotin-streptavidin binding (cell 2,2).

Chapter 5

Protein Detection using Aptamers

This chapter presents the application of the differential micromechanical sensor to protein detection by using a novel receptor technology: *aptamers*. First, an introduction is presented on aptamers, their significance as receptor molecules, and their synthesis process. Application of the sensor to two different aptamer-ligand systems is presented. First, the proof-of-principle for the use of aptamers on cantilevers is demonstrated via aptamer-thrombin binding. Then, a more detailed study involving concentration dependence and detection limits is presented on the detection of *taq* DNA polymerase using specifically selected aptamers. The experimental procedure is covered including the functionalization of the cantilever surfaces with aptamers and the preparation and injection of target molecule solutions. Experimental results concerning specificity and concentration dependence are presented and discussed.

5.1 Aptamers

A key element of the differential micromechanical sensor is the receptor molecules that can specifically recognize and bind to target molecules in the surrounding solution. One class of molecules that can bind to many kinds of target molecules are antibodies. Antibodies are a part of complex immune systems and are produced specifically to recognize foreign elements or antigens that enter into the organism, and tag them for destruction by other immune system members such as macrophages. Antibodies can

bind to their targets with extreme sensitivity, i.e., binding affinities that are as low as femtomolars [50].

However, producing antibodies generally requires a biological host. If the DNA sequence that encodes a specific antibody is known, that sequence can be expressed in a cell such as *E.coli*. The cell in turn transcribes the DNA, translates the resulting RNA and forms the corresponding antibody. The cell can then be lysed, and the antibodies can be extracted for further use. Many antibodies that are commercially available at chemical companies are produced this way. However, to have the genetic information about a specific antibody, that antibody must be known in the first place. It is not possible to have *a priori* knowledge of an antibody that is specific to a random antigen (or target molecule such as protein). The best method to find this out is to introduce the specific antigen into a sophisticated organism and trigger its immune response to produce specific antibodies. It is possible to purchase antibodies against many antigens that have been developed in goats, donkeys, rabbits etc.

The ability to produce receptor molecules without the need of a biological host is highly desirable, since coupling them with surfaces can potentially result in biosensors that are completely man-made. An emerging class of receptors that does not require any biological environment is aptamers. Aptamers are single-stranded nucleic acids (RNA or DNA) capable of binding tightly and specifically to their targets [51, 52]. They are selected from a pool of combinatorial oligonucleotide libraries by a process known as *in vitro* selection [50]. This process is also known as *systematic evolution of ligands by exponential enrichment* (SELEX). As the name implies, SELEX mimics the process of natural evolution. The specific target molecule is introduced into a pool of up to 10^{15} single-stranded DNA strands with different sequences. Each strand is usually 30 to 60 nucleotides long. The strands that bind to the target molecules are isolated, and preferentially amplified via conventional techniques such as PCR. Over multiple rounds of selection and amplification, only the *fittest* aptamers remain. By this technique, it is possible to isolate receptor molecules that can bind to target molecules with high specificity and sensitivity.

Aptamers can bind to an amazingly wide range of targets, ranging from metal

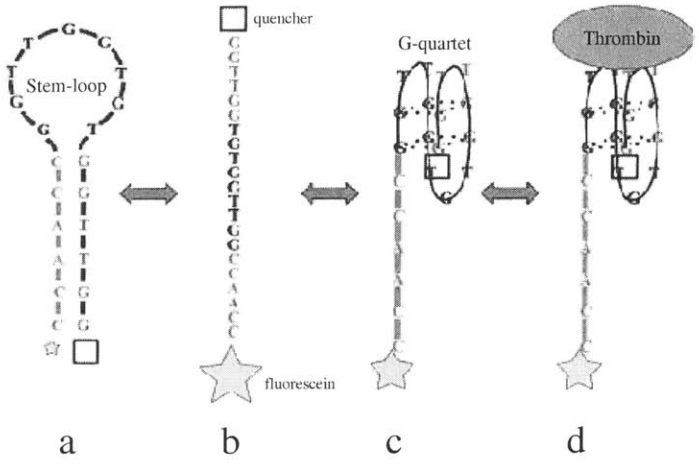

Figure 5-1: A thrombin-binding aptamer and its conformation change to bind to the target protein.

ions to complex cellular structures, to whole cells and to viral particles. Also, since aptamers are selected *in vitro*, they can potentially be raised against pathogens, toxins, biological warfare agents, and other targets that prove problematic for *in vivo* immunization procedures. Also, because of their simple structure, sensor layers based on aptamer receptors can be regenerated more easily than antibody-based layers, they are more resistant to denaturation and degradation, and have a much longer shelf life [53].

Aptamers can adopt two or more conformations, one of which allows binding to a target molecule. Fig. 5-1 illustrates an aptamer selected to bind to thrombin [54]. Thrombin is a protein that plays an important role in blood coagulation. The aptamer is engineered to have complementary ends that hybridize in the absence of thrombin to form a *stem-loop* structure. When the target molecule thrombin is introduced into the solution, the ends dehybridize, and the aptamer strand forms a *g-quartet* structure that allows binding to the thrombin. Binding is detected via fluorescence. One end of the strand is modified with a fluorescein and the other with a quencher. When the aptamer is in the stem-loop conformation, the fluorescein and the quencher are in close proximity, hence, no fluorescence signal is obtained. However, when the aptamer assumes the g-quartet structure, the fluorescein and the quencher are separated, i.e.,

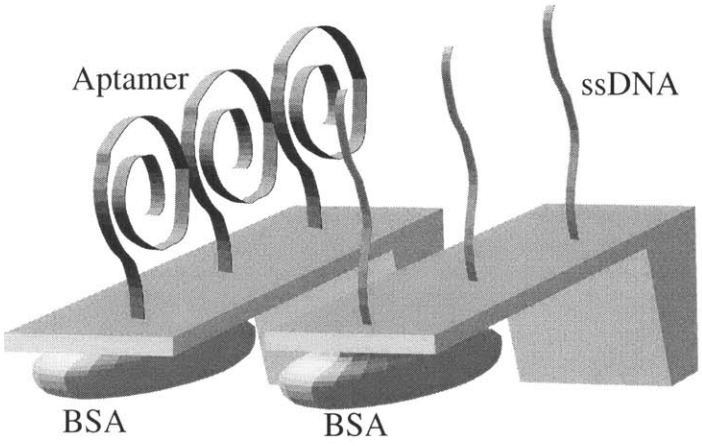

Figure 5-2: Schematic illustrating functionalized surfaces for thrombin detection. Top surfaces are functionalized with aptamers or ssDNA. Bottom surfaces are blocked with BSA.

the fluorescein is no longer quenched and yields a strong signal.

5.2 Micromechanical detection of thrombin

Combining the aptamer-based receptors with cantilever-based sensors has the potential to eliminate the need for labeling molecules (fluorescein and/or radio labels). This thesis study demonstrates for the first time that an aptamer-ligand interaction can cause a surface stress capable of bending a micromachined structure. To perform this, the differential micromechanical sensor was activated with aptamers selected for thrombin.

Fig. 5-2 demonstrates the schematic of the functionalized micromechanical sensor. As usual, one side of the sensor (top surface of each cantilever) was coated with 20 nm of e-beam evaporated gold. The gold-coated side of the sensor cantilever was functionalized with thio-modified aptamers selected for thrombin. The selection process was performed by Scott Knudsen of the Ellington Group at Department of Biochemistry, U.T. Austin. The reference cantilever was blocked with thio-modified ssDNA. Covering the reference surface with ssDNA is much more effective than leaving it

empty. ssDNA makes the reference cantilever as similar to the sensor cantilever as possible. The only difference becomes the affinity of the two surfaces for the specific target molecule. Also, an empty surface introduces the risk of nonspecific binding. The bottom sides (nitride surfaces) of both cantilevers were blocked with BSA. This was done because of the possibility that the two nitride surfaces may slightly differ in their nonspecific affinity for proteins or other molecules in the solution [31]. As demonstrated before, BSA can effectively block a nitride surface and prevent nonspecific adsorption. However, in later experiments that were performed without the BSA blocking, it was found that introducing nonspecific proteins does not cause detectable bending. This suggests that the nitride surfaces of the micromechanical sensor are similar enough in their nonspecific affinity for proteins present in the solution, and that the BSA blocking is not crucial.

Aptamer and ssDNA functionalization were performed immediately following the gold evaporation. Both the aptamer and the ssDNA were 10 μM in water with 50 mM triethylammonium acetate (TEAA) buffer [29]. The device was then placed in a petri dish with a 1 mg/ml BSA solution, and refrigerated at 4 °C overnight. The device was placed in the fluidic cell, and equilibrated in a BSA solution prepared in thrombin binding buffer. A stable baseline was achieved and verified by injecting a BSA solution. Fig. 5-3 shows that injecting a thrombin solution (3 μM in thrombin binding buffer) causes approximately 10 nm of differential cantilever bending. Subsequent injection of a BSA solution did not alter the response, indicating a stable and specific binding.

To demonstrate that the applicability of the micromechanical sensor is not limited to only one specific aptamer (and its corresponding target), a set of experiments were performed with another aptamer selected for *taq* DNA polymerase. Experiments with *taq* also involve investigation of concentration dependence and selectivity, i.e., the ability to detect the target molecule in the presence of a complex nonspecific mixture.

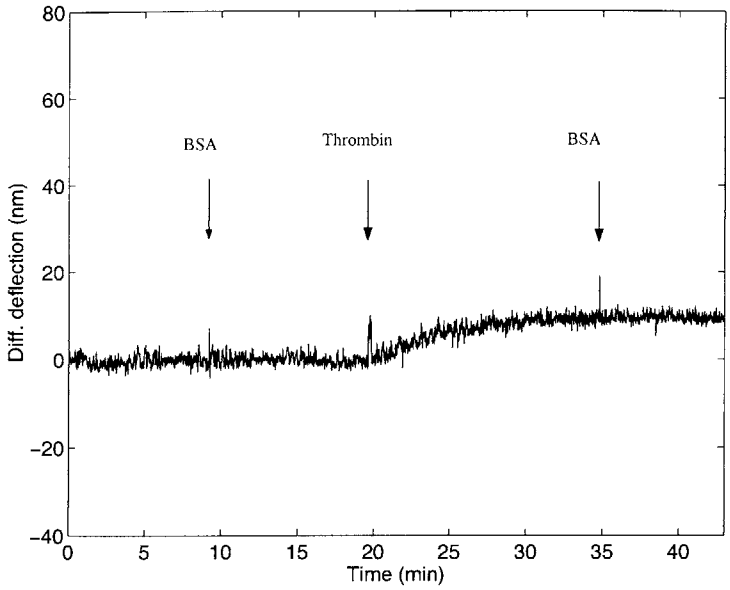

Figure 5-3: Micromechanical detection of thrombin using aptamers. Injecting BSA solution causes no differential response, whereas injecting thrombin solution causes clear differential bending.

5.3 *Taq* DNA polymerase detection

Taq DNA polymerase is retrieved from the thermophylic bacteria *Thermus Aquaticus*. The bacteria live in warm environments and can withstand temperatures up to 95 °C. Due to its thermal stability, *taq* DNA polymerase, which will be simply referred to as *taq* from now on, is commonly used in the polymerase chain reaction (PCR).

The conformational structure of the thrombin aptamer is well understood. This is not necessarily the case for all aptamers. For instance, the shape that the *taq* aptamer assumes to allow binding to its target is not known. One strength of the SELEX process is that it does not require this knowledge, since the aptamers are *selected* from large pools of randomly sequenced oligonucleotides, not designed based on conformational knowledge[1]. Specifically selected aptamers bind to *taq* with very high affinity (~10 pM) [55].

One common method for detecting aptamer-ligand interactions is the *filter binding assay*. It is also used to detect the specific aptamer-*taq* binding. The basics of the

[1]However, the aptamer can be modified once the basic selection is completed.

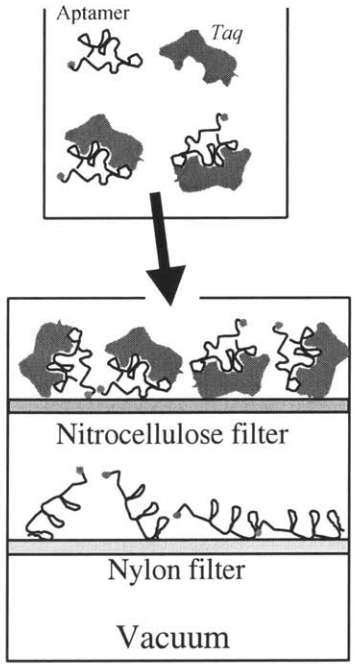

Figure 5-4: *Taq* DNA polymerase detection using filter binding assay.

method are illustrated by Fig. 5-4. In this method, the aptamers are radio-labeled, and allowed to interact with the *taq* molecules. After ample time to complete the binding reaction, the mixture is pushed through a double-filter based assembly. The push-through is assisted by a vacuum in the bottom of the assembly. The first filter is a nitrocellulose filter. Bound receptor-ligand pairs (in this case aptamer-*taq* pairs) cannot pass through the holes of the nitrocellulose filter. However, the unbound free aptamers are small and flexible enough to pass through the nitrocellulose filter, and stick to the nylon filter beneath. The setup is then disassembled, and surfaces of both filters are imaged for strength of radioactive emission. The ratio of the signal from the nitrocellulose filter (bound aptamers) to the sum of the signals from both filters (bound+unbound aptamers) yields the *binding fraction* of aptamers.

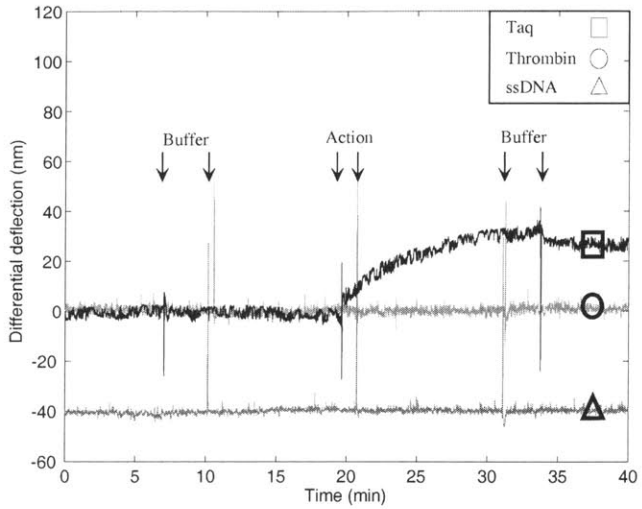

Figure 5-5: *Taq* DNA polymerase detection and control experiments. *Taq* injection yields binding response. Thrombin injection causes no signal. Both cantilevers functionalized with ssDNA (intentionally plotted with -40 nm DC offset for clarity) yields no response.

5.4 Micromechanical detection of *taq*

To perform the *taq* binding experiment, the micromechanical sensor was functionalized very similarly to the illustration in Fig. 5-2, except the bottom surfaces were not blocked with BSA. Again, the top surfaces of both cantilevers were coated with 20 nm of gold, and the functionalization was performed immediately after the gold deposition. The sensor cantilever's gold-coated surface was functionalized with thio-modified aptamers selected for *taq*, and the reference cantilever was again blocked with ssDNA.

First, the specificity of the aptamer-protein binding was tested by exposing the sensor to two different protein solutions: 1. thrombin, which is a protein that is not expected to interact with the *taq* aptamer, 2. *taq*, which is the protein that the immobilized aptamer has been selected for. Fig. 5-5 shows an overlay of the sensor's response to both proteins. The device was placed in the fluidic chamber and equilibrated in *taq* binding buffer. Subsequent injection of buffer revealed negligible differential signal, and served to verify the stability of the baseline. As expected,

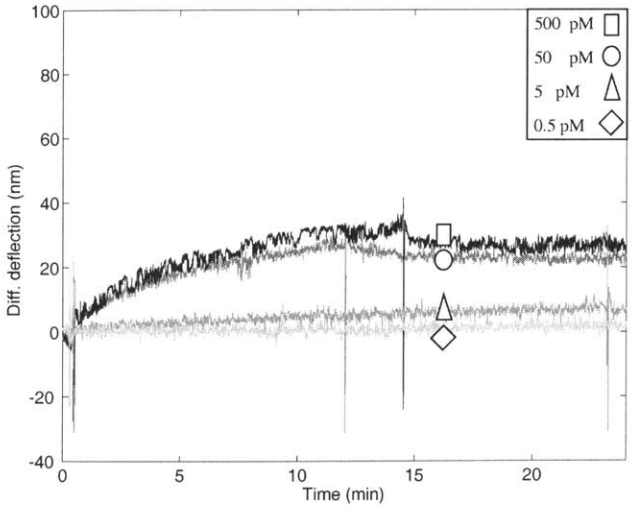

Figure 5-6: Time domain representation of sensor response to various concentrations of *taq* injection. Reaction was denatured with urea before each injection.

injecting a 75 nM thrombin solution revealed no differential cantilever bending. The experiment was then repeated, this time by injecting a 500 pM *taq* solution into the fluidic chamber. This resulted in 32 nm of differential cantilever bending. Subsequent buffer injection caused a slight decrease in the signal, possibly because the nonspecifically bound ligands were washed away.

Fig. 5-5 also shows the response to *taq*, when both the sensor and the reference cantilever are functionalized with ssDNA. This response was intentionally plotted with -40 nm of DC offset for clarity. To perform this experiment, the gold layer of the device was stripped by aqua-regia (3:1 HCl:HNO_3), a fresh gold layer was deposited, and the functionalization was performed by exposing both cantilevers to the ssDNA solution. Again, the device was placed in the fluidic cell, and equilibrated in buffer. As expected, injecting a *taq* solution did not cause any differential bending. This is because *taq* does not interact with the ssDNA on either cantilever, or it interacts nonspecifically with each cantilever by the same amount.

The experiment was performed at various *taq* concentrations. Fig. 5-6 illustrates the sensor response to 4 different *taq* concentrations over time. After each experiment, the reaction was denatured by injecting a 7M urea solution into the fluidic chamber

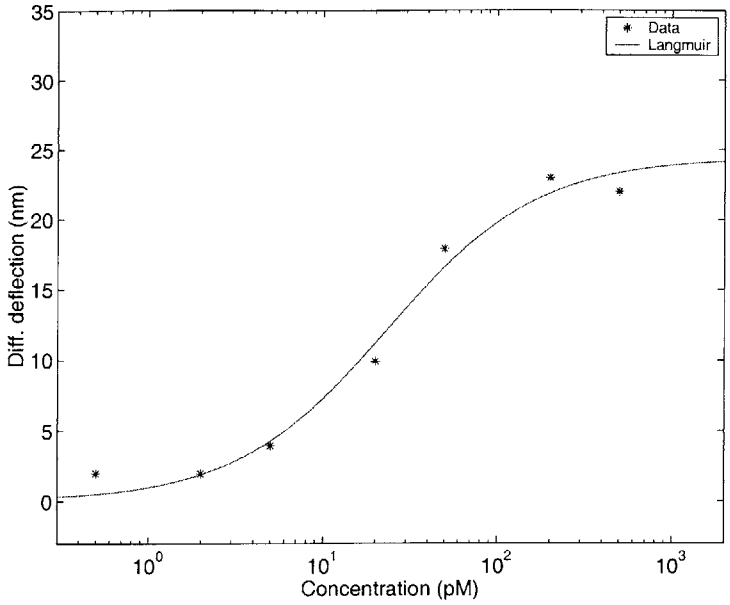

Figure 5-7: Sensor response to increasing concentration of *taq* and the fit for the Langmuir isotherm. *Taq* solutions were sequentially injected with increasing concentration, without any denaturation steps.

[56]. Higher concentrations reveal larger differential signals.

The concentration dependence of the system was also investigated by performing *taq* injections sequentially with increasing concentration, and without the use of urea. This method is not desirable to observe binding kinetics since each *taq* injection acts on a surface that is partially occupied due to the previous injection. Performing injections with alternating urea washes enables to start from a relatively unoccupied or fresh surface, and hence is more desirable for measuring reaction kinetics. However, the complete effect of urea on the surface is not known, i.e., the urea wash performed between target injections does not guarantee a perfectly fresh surface. Hence, performing an experiment by only increasing *taq* concentration and measuring the resulting steady-state deflection may yield a more reliable representation of surface coverage.

Fig. 5-7 shows the steady-state differential deflection vs. *taq* concentration (in logarithmic scale). Also shown is a least squares Langmuir isotherm fit. The Langmuir

isotherm describes an ideal first-order receptor-ligand binding reaction [57]:

$$\Delta z = \frac{\Delta z_{max}}{1 + \frac{K_d}{L}}. \tag{5.1}$$

Here, Δz is the generic sensor response: in this case, the differential cantilever deflection. Δz_{max} is the maximum sensor response, corresponding to saturation. L is the ligand concentration in pM. K_d is the dissociation constant of the reaction, i.e., the ligand concentration which causes 50% of the receptors to be occupied. The fit to the plotted data points revealed a K_d of 23 pM and a Δz_{max} of 24 nm. The K_d extracted from the measurements performed *in solution* using the filter binding assay is 9 pM [58]. Considering that the concentration experiments sweep over a large range (3-4 orders of magnitude), the difference between the two K_d values is quite small. That being said, the larger K_d value of the micromechanical system is plausible, since in this system the receptor molecules are immobilized on the surface as opposed to being free molecules in solution. Immobilized molecules cannot move around to find a free target molecule, and in general may have less freedom to change conformation. Hence, the need for a larger concentration for a given amount of binding is understandable.

Next, the selectivity of the system was investigated via detecting *taq* in the presence of a complex protein mixture[2]. *E.coli* (*Escherichia coli*) cell lysate was used as the complex protein mixture[3]. The cell lysate contains over 10,000 proteins and many other biomolecules.

Fig. 5-8 shows the results of this experiment. The device was prepared and functionalized as described before, placed in the fluidic cell and equilibrated in *taq* binding buffer. The baseline was again verified by a buffer injection. Injecting a cell lysate solution caused no differential response. Whereas, injecting the same cell lysate combined with *taq* resulted in ~20 nm of differential sensor response.

[2]This experiment was performed at a later time, using a separate sensor (same geometry as the one used for previous experiments).

[3]Bacteria were cultured and lysed by John Albeck and Suzanne Gaudet of Sorger Group at MIT Dept. of Biology.

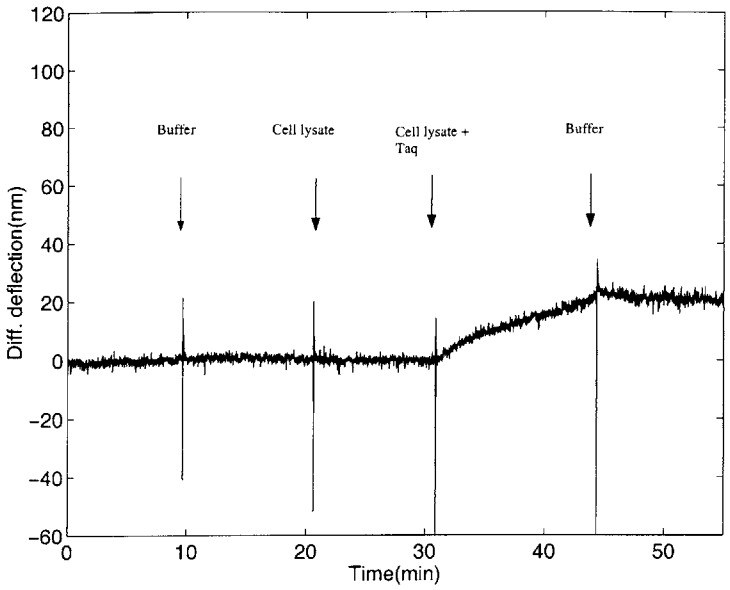

Figure 5-8: *Taq* detection in the presence of a complex protein mixture. Average protein concentration of cell lysate: 700 pM. Taq concentration: 50 pM.

5.5 Verification using quartz crystal microbalance

The *taq* experiment was verified using a quartz crystal microbalance (QCM) system. This was done to independently confirm the specific aptamer-ligand binding on a surface that is as similar to the cantilever surface as possible.

A quartz crystal microbalance (QCM) is a mass detector that operates based on a simple dynamic principle. Mass addition to the surface of the crystal reduces its resonance frequency. Knowledge of the change in the resonance frequency enables quantification of the mass adsorbed onto the crystal surface [53]:

$$\Delta m = -\frac{A}{c_f}\Delta f \tag{5.2}$$

with

$$c_f = \frac{2f^2}{\rho_q \nu_q}. \tag{5.3}$$

Here, c_f is the sensitivity constant that depends on the original resonance frequency f of the crystal, density ρ_q of quartz, and the speed of sound in quartz ν_q. A is

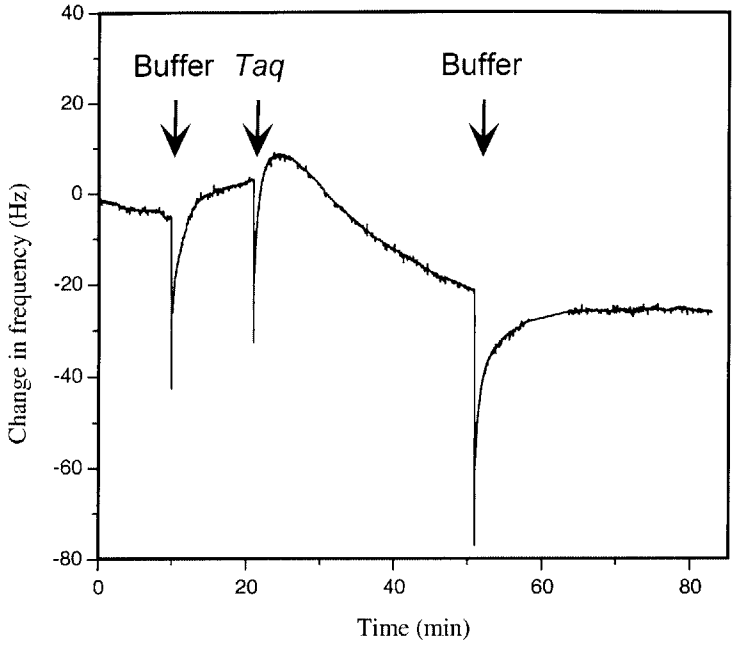

Figure 5-9: *Taq* detection using quartz crystal microbalance.

the surface area of the crystal, Δm and Δf are changes in mass and the resonance frequency of the crystal respectively. Quartz crystals are usually coated with gold and hence, be functionalized with thio-modified receptor molecules. They can also be enclosed in commercially available fluidic cells to be used for detecting adsorption of biomolecules. QCM systems are extremely sensitive to temperature changes and are generally used with a temperature control unit. To perform the experiment, a Maxtek QCM detection system was used. A 9 MHz gold-coated quartz crystal[4] was functionalized with the same *taq* aptamers used to functionalize the micromechanical sensor. The gold surface was cleaned with a piranha solution and copiously washed with nanopure water before the functionalization. The aptamer solution was then pipetted onto the gold-coated surface of the crystal and allowed to stay on the surface for about 30 minutes. The crystal was then washed and placed into a Maxtek teflon fluidic cell. The fluidic cell was placed in a glass jar which was connected to a temperature control unit.

The system was allowed to equilibrate for a few hours. The measurement exhibited

[4]Maxtek 149255-1

a significant amount of linear drift, possibly due to not being differential. At the end of the experiment, the linear drift was subtracted from the data set. Fig. 5-9 shows the drift-corrected response of the QCM system[5]. Despite the temperature control unit, the system is not completely stable and exhibits long transients after injections. Injecting a 50 pM *taq* solution caused about 20 Hz reduction in the resonance frequency of the cantilever. Using 5.2 and 5.3 (with $\rho_q = 2648$ kgm^3, and $\nu_q = 3340$ ms^{-1} and $A = 1.27$ cm^2) yields a mass change of 139 ng. For *taq* with a molecular weight of 94 kDa, this corresponds to about 7,000 bound molecules per μm^2.

Since the surfaces of both the QCM and the micromechanical sensor are gold, this can also be conceived as a rough estimate for the number of molecules that bind to the cantilever during an experiment. This is only a rough estimate because the two surfaces are not exactly the same. The gold on the cantilevers was deposited on silicon nitride with titanium as an adhesion layer, whereas the gold on the crystal was put on quartz with chromium as the adhesion layer. More importantly, the gold on the cantilevers was freshly deposited, and functionalized immediately following the deposition, whereas the gold on the crystal was not fresh and was cleaned with piranha[6]. Hence, the two gold surfaces are not identical and the calculated number of molecules cannot directly apply to the cantilever-based sensor.

The QCM experiment was quite useful to verify a specific aptamer-ligand binding reaction, to observe the difficulties of non-differential or absolute detection and to have a rough estimate of the number of molecules that bind to the cantilever surface during the experiment.

[5]At time=60 min. data acquisition stopped for 5 minutes. Software joins each two points with a line to generate plot.

[6]The gold on the crystal is deposited with a specific pattern, and cannot easily be stripped and re-deposited to form the same shape.

Chapter 6

Conclusions

6.1 Conclusions

A new micromechanical label-free biosensor has been presented. The sensor provides a signal that directly represents the difference between the responses of two surfaces: one that allows binding of specific molecules, and an adjacent one that does not. The sensor is constituted by two adjacent cantilevers that bend in response to surface stresses generated by binding of biomolecules. The specific design allows the direct detection of the relative, i.e., differential bending between the two cantilevers. Hence, the two cantilevers form a sensor-reference pair, and the disturbances that influence both cantilevers are suppressed.

The direct differential bending is detected by interdigital fingers located between the tips of the two cantilevers. The fingers form a diffraction grating, which produces a pattern composed of several modes when illuminated by a laser beam. The intensities of the modes change as one cantilever deflects with respect to the other. The dependence of the modal intensities on the relative deflection is known analytically. Hence, the intensity of one of the modes can be measured by a photodetector and can be directly calibrated for the relative deflection in nanometers.

The geometry of the sensor was appropriately designed so that each cantilever can be functionalized separately by simply inserting it into a commercially available pipette to deposit receptor molecules. The specific geometry was realized by forming

thick support structures that were fabricated simultaneously with the flexible cantilevers. The overall structure was fabricated out of silicon nitride using standard micromachining techniques.

The characterization of the sensor showed that changes in both temperature and the chemical properties of the solution can induce cantilever bending, and that these effects are successfully suppressed by the inherently differential nature of the sensor. Noise analysis showed that at high frequencies (above 40 Hz), the resolution of the sensor is only limited by its sub-angstrom level thermomechanical noise. Hence, for applications above 40 Hz, the precision of deflection measurement is less than the size of a single atom. However, the intended application of the sensor is biomolecular binding reactions, most of which occur over minutes or tens of minutes. In the corresponding frequency range, the sensor is limited by 1/f-type low-frequency noise. It was shown that at frequencies below 1 Hz, differential detection reduces the low frequency noise by up to an order of magnitude. It was also shown that most of the low-frequency noise is due to cantilever deflection and not the optical detection system or the electronic components of the experimental setup.

The sensor's application to protein detection was tested by a model biotin-streptavidin reaction, and verified on an identical surface by fluorescence microscopy. The sensor was also used to perform protein detection with aptamers. It was shown for the first time that an aptamer-protein reaction generates a surface stress capable of bending a micromachined cantilever. For a specific aptamer-protein reaction, it was shown that the concentration dependence of the sensor response follows a Langmuir isotherm-type behavior, and that detecting sub-picomolar concentrations is possible.

6.2 Recommendation for future work

Cantilever-based sensors are capable of performing sensitive detection of biomolecules without the use of labels. However, much is yet to be understood about the mechanism responsible for cantilever bending. A thorough understanding of intermolecular forces and their dependence on surface properties can enable accurate modeling and

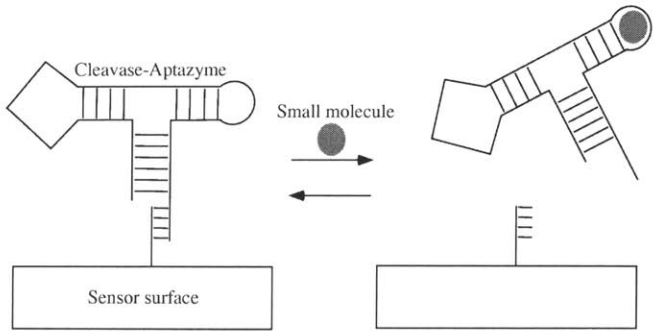

Figure 6-1: Small molecule detection using aptazymes. Small molecule is detected via the activity of the much larger aptazyme.

simulation of the sensing system. This can in turn enable optimization of cantilever geometries and surfaces for high sensitivity detection.

Cantilever-based sensors can also be used to investigate protein conformations. Due to their ability to detect surface stress, cantilever-based sensors can reveal valuable information about unfolding of densely-packed proteins. This information cannot easily be obtained with other sensors that simply detect the presence or mass of bound molecules.

Another area of improvement is integration with microfluidics and packaging. An important advantage of the developed method is its low sensitivity to ambient disturbances and its scalability. A portable device with an array of sensors is one of the ultimate goals that can be achieved with the interferometric micromechanical sensor.

Finally, much is yet to be achieved on the integration of biosensors with aptamers. Aptamers enable not only label-free protein sensing, but also small molecules. Small molecules, i.e., molecules that are much smaller than proteins (e.g. a single DNA base, an ATP molecule, a drug molecule) are very important and their direct detection is challenging. Fig. 6-1 demonstrates small molecule detection by aptazymes on the surface of a generic sensor. The small molecule triggers the activity of an aptamer-based enzyme, i.e., *aptazyme* which in turn cleaves itself from the surface tether. Hence, the small molecule is indirectly detected via a much larger molecule. Integrating this method with the micromechanical sensor can lead to significant advances in label-free

small molecule sensing.

Appendix A

Chemicals

1. BSA: Bovine serum albumin. Sigma A-0281
2. BSA-FITC: FITC-labeled bovine serum albumin. Sigma A-9771
3. bBSA: Biotin-labeled bovine serum albumin. Sigma A-8549
4. SA: Streptavidin. Sigma S-4762
5. SA-FITC: FITC-labeled streptavidin S-3762
6. PEG: Thiolated polyethyleneglycol No. 12 750-4 Rapp Polymere GmbH, Germany
7. PBS: Prepared by dissolving one tablet of Sigma P-4417 in 200 mL of water.
8. Thrombin aptamer (thiolated)

HS(CH2)6TTTTTTTTTTGGTTGGTGTGGTTGG

9. *Taq* aptamer (thiolated)

HS(CH2)6TTTTTTGGCGGAGCGATCATCTCAG-

-AGCATTCTTAGCGTTTTGTTCTTGTGTATGA

10. Single-stranded DNA (thiolated)

HS(CH2)6GCGACTGGACATCACGAG

11. Thrombin: Sigma T-4648
12. *Taq* DNA polymerase: Sigma D-1806
13. Thrombin binding buffer: 20 mM Tris-Acetate, 140 mM NaCl, 5mM KCl, 1 mM CaCl, 1 mM $MgCl_2$
14. *Taq* binding buffer: 10 mM Tris-HCl (pH 8.3), 50 mM KCl, 2.5 mM $MgCl_2$

Bibliography

[1] L. Kricka. Nucleic acid detection technologies - labels, strategies and formats. *Clinical Chemistry*, 45(4):453–458, January 1999.

[2] H.M. Haake, A. Schuts, and G. Gauglitz. Label-free detection of biomolecular interaction by optical sensors. *Fresenius Journal of Analytical Chemistry*, 366:576–585, 2000.

[3] H.J. Trurnit. Ellipsometry. *Archives of Biochemistry and Biophysics*, 47:251–271, July 1953.

[4] B. Liedberg, C. Nylander, and I Lundstrom. Surface plasmon resonance for gas detection and biosensing. *Sensors and Actuators*, 4:299–304, June 1983.

[5] D.G. Myszka, M.D. Jonsen, and B.J. Graves. Equilibrium analysis of high affinity interactions using BIACORE. *Analytical Biochemistry*, 265:326–330, July 1998.

[6] *Polymer Handbook*. Number 469 in VII. Wiley, third edition, September 1989.

[7] BIACORE AB. *Technical note 1 BR9001-15*, April-May 2001. www.biacore.com.

[8] C.K. O'Sullivan and G.G. Guilbault. Commercial quartz crystal microbalances - theory and applications. *Biosensors and Bioelectronics*, 14:663–670, August 1999.

[9] T.P. Burg and S.R. Manalis. Suspended microchannel resonators for biomolecular detection. *Applied Physics Letters*, 83(13):2698–2700, September 2003.

[10] R.J. Chen, S. Bangsaruntip, K.A. Drouvalakis, N.W.S. Kam, M. Shim, Y. Li, P.J. Utz, and H. Dai. Noncovalent functionalization of carbon nanotubes for highly specific electronic biosensors. *Proceedings of the National Academy of Sciences*, 100(9):4984–4989, April 2003.

[11] D.G. Hafeman, J.W. Parce, and H.M McConnell. Light-addressable potentiometric sensor for biochemical systems. *Science*, 240(4856):1182–1185, May 1988.

[12] L. Bousse and P. Bergveld. On the impedance of the silicon dioxide/electrolyte interface. *Journal of Electroanalytical Chemistry*, 152:25–39, January 1983.

[13] S.R. Manalis, E.B. Cooper, P.F. Indermuhle, P. Kernen, P. Wagner, D.G. Hafeman, S.C. Minne, and C.F. Quate. Microvolume field-effect pH sensor for the scanning probe potentiometer. *Applied Physics Letters*, 76(8):1072–1074, February 2000.

[14] E.B. Cooper, J. Fritz, G. Wiegand, P. Wagner, and S.R. Manalis. Robust microfabricated field-effect sensor for monitoring molecular adsorption in liquids. *Applied Physics Letters*, 79(23):3875–3877, December 2001.

[15] J. Fritz, E.B. Cooper, S. Gaudet, P. Sorger, and S.R. Manalis. Electronic detection of DNA by its intrinsic molecular charge. *PNAS*, 99(22):14142–14146, October 2002.

[16] A.W. Adamson. *Physical Chemistry of Surfaces.* Wiley, New York, 1990.

[17] G. Lang and K.E. Heusler. Problems related to the specific surface energy of solid electrodes. *Journal of Electroanalytical Chemistry*, 377(1):1–7, October 1994.

[18] H.J. Butt. A sensitive method to measure changes in the surface stress of solids. *Journal of Colloid and Interface Science*, 180:251–260, 1996.

[19] R. Berger, E. Delamarche, H.P. Lang, C. Gerber, J.K. Gimzewski, E. Meyer, and H.-J. Guntherodt. Surface stress in the self-assembly of alkanethiols on gold. *Science*, 276:2021–2023, June 1997.

[20] R. Raiteri, H.J. Butt, and M. Grattarola. Changes in surface stress at the liquid/solid interface measured with a microcantilever. *Electrochimica Acta*, 46:157–163, 2000.

[21] H-.F. Ji, K.M. Hansen, Z. Hu, and T. Thundat. Detection of pH variation using modified microcantilever sensors. *Sensors and Actuators B*, 72:233–238, 2000.

[22] J. Fritz, M.K. Baller, H.P. Lang, T. Strunz, E. Meyer, H.-J. Guntherodt, E. Delamarche, C. Gerber, and J.K. Gimzewski. Stress at the solid-liquid interface of self-assembled monolayers on gold investigated with a nanomechanical sensor. *Langmuir*, 16:9694–9696, October 2000.

[23] L.A. Pinnaduwage, J.E. Boiadjiev, J.E. Hawk, and T. Thundat. Sensitive detection of plastic explosives with self-assembled monolayer-coated microcantilevers. *Applied Physics Letters*, 83(7):1471–1473, August 2003.

[24] M.F. Hagan, A. Majumdar, and A.K. Chakraborty. Nanomechanical forces generated by surface grafted DNA. *Journal of Physical Chemistry B*, 106:10163–10173, July 2002.

[25] G. Wu, H. Ji, K. Hansen, T. Thundat, R. Datar, R. Cote, M. Hagan, A. Chakraborty, and A. Majumdar. Origin of nanomechanical cantilever motion generated from biomolecular interactions. *PNAS*, 98:1560–1564, February 2001.

[26] K.M. Hansen, H.-F. Ji, G. Wu, R.H. Datar, R.J. Cote, A. Majumdar, and T. Thundat. Cantilever-based optical deflection assay for discrimination of DNA single-nucleotide mismatches. *Analytical Chemistry*, 73:1567–1571, April 2001.

[27] G. Wu, R.H. Datar, K.M. Hansen, T. Thundat, , R.J. Cote, and A. Majumdar. Bioassay of prostate-specific-antigen (psa) using microcantilevers. *Nature Biotechnology*, 19:856–860, September 2001.

[28] A. Subramanian, P.I. Oden, S.J. Kennel, K.B. Jacobson, R.J. Warmack, T. Thundat, and M.J. Doktycz. Glucose biosensing using an enzyme-coated microcantilever. *Applied Physics Letters*, 81:385–387, July 2002.

[29] J. Fritz, M.K. Baller, H.P. Lang, T. Strunz, E. Meyer, H.-J. Guntherodt, E. Delamarche, C. Gerber, and J.K. Gimzewski. Translating biomolecular recognition into nanomechanics. *Science*, 288:316–318, April 2000.

[30] R. McKendry, J. Zhang, Y. Arntz, T. Strunz, M. Hegner, H.P. Lang, M.K. Baller, U. Certa, E. Meyer, H.-J. Guntherodt, and C. Gerber. Multiple label-free biodetection and quantitative DNA-binding assays on a nanomechanical cantilever array. *PNAS*, 99(15):9783–9788, July 2002.

[31] Y. Arntz, J.D. Seelig, H.P. Lang, J. Zhang, P. Hunziker, J.P. Ramseyer, E. Meyer, M. Hegner, and C. Gerber. Multiple label-free biodetection and quantitative DNA-binding assays on a nanomechanical cantilever array. *Nanotechnology*, 14:86–90, January 2003.

[32] G.Y. Chen, T. Thundat, E.A. Wachter, and R.J. Warmack. Adsorption-induced surface stress and its effects on resonance frequency of cantilevers. *Journal of Applied Physics*, 77:3618–3623, April 1995.

[33] A.M. Moulin, S.J. O'Shea, R.A. Bradley, P. Doyle, and M.E. Welland. Measuring surface induced conformational changes in proteins. *Langmuir*, 15:8776–8779, September 1999.

[34] G.G. Stoney. The tension of metallic films deposited by electrolysis. *Proceedings of the Royal Society of London*, 82:172–175, February 1909.

[35] R. Raiteri, M. Grattarola, H.J. Butt, and P. Skladal. Micromechanical cantilever-based biosensors. *Sensors and Actuators*, 79:115–126, May 2001.

[36] J. Lai, T. Perazzo, T. Shi, and A. Majumdar. Optimization and performance of high-resolution micro-optomechanical thermal sensors. *Sensors and Actuators-A*, 58:113–119, 1997.

[37] L.A. Nagahara, T. Thundat, and S.M. Lindsay. Preparation and characterization of STM tips for electrochemical studies. *Review of Scientific Instruments*, 60(10):3128–3130, October 1989.

[38] G.G. Yaralioglu, A. Atalar, S.R. Manalis, and C.F. Quate. Analysis and design of an interdigital cantilever as a displacement sensor. *Journal of Applied Physics*, 83:7405–7415, June 1998.

[39] S.R. Manalis, S.C. Minne, A. Atalar, and C.F. Quate. Interdigital cantilevers for atomic force microscopy. *Applied Physics Letters*, 69:3944–3946, December 1996.

[40] S.C. Minne, S.R. Manalis, and C.F. Quate. *Bringing Scanning Probe Microscopy up to Speed.* Microsystems. Kluwer Academic Publishers, Norwell, Massachusetts, USA, 1999.

[41] C.A. Savran, A.W. Sparks, J. Sihler, J. Li, W-.C. Wu, D.E. Berlin, T.P. Burg, J. Fritz, M.A. Schmidt, and S.R. Manalis. Fabrication and characterization of a micromechanical sensor for differential detection of nanoscale motions. *Journal of Microelectromechanical Systems*, 11(6):703–708, December 2002.

[42] W.T. Thompson and M.D. Dahleh. *Theory of Vibrations with Applications.* Prentice Hall, New Jersey, fifth edition, 1998.

[43] J.R. Barnes, R.J. Stephenson, C.N. Woodburn, S.J. O'Shea, M.E. Welland, T. Rayment, J.K. Gimzewski, and Ch. Gerber. A femtojoule calorimeter using micromechanical sensors. *Review of Scientific Instruments* , 65(12):3793–3798, December 1994.

[44] J. Tamayo, A.D.L. Humphris, and M.J. Miles. Piconewton regime dynamic force microscopy in liquid. *Applied Physics Letters*, 77(4):582–584, July 2000.

[45] D.L. Harame, L.J. Bousse, J.D. Shott, and J.D. Meindl. Ion-sensing devices with silicon nitride and borosilicate glass insulators. *IEEE Transactions on Electron Devices*, 34(8):1700–1707, August 1987.

[46] S.D. Senturia. *Microsystem Design.* Kluwer Academic Publishers, Massachusetts, 2001.

[47] C.A. Savran, T.P. Burg, J. Fritz, and S.R. Manalis. Microfabricated mechanical biosensor with inherently differential readout. *Applied Physics Letters*, 83(8):1659–1661, August 2003.

[48] R.C. Weast and M.J. Astle. *CRC Handbook of Chemistry and Physics.* CRC, Boca Raton, Florida, 1979.

[49] Hamad-Schifferli K., J.J. Schwartz, A.T. Santos, S. Zhang, and J.M. Jacobson. Remote electronic control of DNA hybridization through inductive coupling to an attached metal nanocrystal antenna. *Nature*, 415:152–155, January 2002.

[50] A.D. Ellington. *Nucleic acids for reagentless biosensors*, chapter 12. Unpublished book chapter.

[51] C. Tuerk and L. Gold. Systematic evolution of ligands by exponential enrichment: RNA ligands to bacteriophage T4 DNA polymerase. *Science*, 294:2345–131, August 2001.

[52] A.D. Ellington and J.W. Szostak. In vitro selection of RNA molecules that bind specific ligands. *Nature*, 346:818–822, August 1990.

[53] M. Liss and B. Petersen. An aptamer-based quartz crystal protein biosensor. *Analytical Chemistry*, 74(17):4488–4495, September 2002.

[54] N. Hamaguchi, A. Ellington, and M. Stanton. Aptamer beacons for the direct detection of proteins. *Analytical Biochemistry*, 294:2345–131, June 2001.

[55] Y. Lin and S.D. Jayasena. Inhibition of multiple thermostable DNA polymerases by a heterodimeric aptamer. *Journal of Molecular Biology*, 271(8):100–111, 1997.

[56] S.M. Knudsen. Personal communication.

[57] R.A. Copeland. *Enzymes A Practical Introduction to Structure, Mechanism and Data Analysis.* Wiley-VCH, New York, 2000.

[58] C.A. Savran, S.M. Knudsen, A.D. Ellington, and S.R. Manalis. Micromechanical detection of proteins using aptamer-based receptor molecules. *Analytical Chemistry.* in preparation.